Artificial Intelligence-based multi-objective optimization of a solar-driven system for hydrogen production with integrated oxygen and power Co-generation across different climates

International Journal of Hydrogen Energy 184 (2025) 151880

Contents lists available at ScienceDirect

International Journal of Hydrogen Energy

journal homepage: www.elsevier.com/locate/he

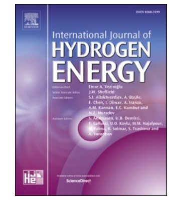

Artificial Intelligence-based multi-objective optimization of a solar-driven system for hydrogen production with integrated oxygen and power Co-generation across different climates

Ehsanolah Assareh [a,b,c], Behzad Rismanchi [a], Nima Izadyer [c,d,*], Ali Bedakhanian [b], Elmira Jamei [c,d], Jagadeesh Kumar Alagarasan [e,**]

[a] Renewable Energy and Energy Efficiency Group, Department of Infrastructure Engineering, Faculty of Engineering and IT, The University of Melbourne, Australia
[b] Strategic Research Institute (SRI), Asia Pacific University of Technology and Innovation (APU), Technology Park, Malaysia, Kuala Lumpur, Malaysia
[c] Built Environment and Engineering Program, College of Sport, Health and Engineering (CoSHE), Victoria University, Melbourne, VIC, 3011, Australia
[d] Institute for Sustainable Industries and Liveable Cities, Victoria University, Melbourne, VIC, 3011, Australia
[e] Department of Chemistry, Faculty of Science, Technology and Architecture (FoSTA), Manipal University Jaipur, Jaipur, 303007, Rajasthan, India

ARTICLE INFO

Keywords:
Artificial intelligence optimization
Climate-responsive design
Hydrogen production
Multi-generation energy systems
Proton exchange membrane electrolyzer
Solar thermal energy

ABSTRACT

This study develops and optimizes a solar-powered system for hydrogen generation with oxygen and power co-products, addressing the need for efficient, scalable carbon-free energy solutions. The system combines a linear parabolic collector, a Steam Rankine cycle, and a Proton Exchange Membrane Electrolyzer (PEME) to produce electricity for electrolysis. Thermodynamic modeling was accomplished in Engineering Equation Solver, while a hybrid Artificial Intelligence (AI) framework combining Artificial Neural Networks and Genetic Algorithms in Statistica, coupled with Technique for Order Preference by Similarity to Ideal Solution (TOPSIS) decision support, optimized technical and economic performance. Optimization considered seven key decision variables, covering collector design, thermodynamic inputs, and component efficiencies. The optimization achieved energy and exergy efficiencies of 30.83 % and 26.32 %, costing 47.02 USD/h and avoiding CO_2 emissions equivalent to 190 USD/ton. Economic and exergy analyses showed the solar and hydrogen units had the highest costs (38.17 USD/h and 9.61 USD/h), with 4503 kWh of exergy destruction to generate 575 kWh of electricity. A case study across six cities suggested that Perth, Bunbury, and Adelaide, with higher solar irradiance, delivered the highest annual power and hydrogen outputs, consistent with irradiance–electrolyzer correlation. Unlike conventional single-site studies, this work delivers a climate-responsive, multi-city analysis integrating solar thermal and PEME within an AI-driven framework. By linking techno-economic performance with quantified environmental value and co-production synergies of hydrogen, oxygen, and electricity, the study highlights a novel pathway for scalable clean hydrogen, measurable CO_2 reductions, and global decarbonization, with future work focused on digital twins and dynamic, uncertainty-aware optimization.

Nomenclature

Symbols		Abbreviations	
A	Collector aperture area [m2]	AEMEs	Anion Exchange Membrane Electrolyzers
A_{ap}	Aperture area of collector [m2]	ANN	Artificial Neural Networks
A_p	Effective collector area (adjusted for efficiency) [m2]	CRF	Capital Recovery Factor

(continued on next column)

(continued)

CP	Specific heat of air and water at constant pressure [kJ/kg.°K]	ELE	Electrolysis
D_{or}	Outer diameter of absorber tube [m]	GA	Genetic Algorithms
D_{ir}	Inner diameter of absorber tube [m]	GHI	Global Horizontal Irradiation

(continued on next page)

* Corresponding author. Built Environment and Engineering Program, College of Sport, Health and Engineering (CoSHE), Victoria University, Melbourne, VIC, 3011, Australia.
** Corresponding author.
E-mail addresses: nima.izadyar@vu.edu.au (N. Izadyer), jaga.jagadeesh1987@gmail.com (J.K. Alagarasan).

https://doi.org/10.1016/j.ijhydene.2025.151880
Received 11 September 2025; Received in revised form 2 October 2025; Accepted 4 October 2025
Available online 11 October 2025

(*continued*)

ex	Specific exergy [kJ/kg.°K]	LCH	Levelized Cost of Hydrogen
$\dot{Ex}$	Exergy transfer rate [kW]	ORC	Organic Rankine Cycle
F1	Collector heat transfer coefficient	PEME	Proton Exchange Membrane Electrolyzer
FR	Heat removal factor of collector	SMR	Steam Methane Reforming
G_b	Beam solar radiation intensity [W/m2]	SRC	Steam Rankine Cycle
h	Specific enthalpy [kJ/kg]	TES	Thermal Energy Storage
hf	Convective heat transfer coefficient [W/m2.°K]	**Greek Symbol**	
k	Index representing inlet/outlet stream	α	Absorptance of absorber surface
$\dot{m}$	Mass flow rate [kg/s]	η	Efficiency
P_0	Ambient pressure [kPa]	η_r	Optical efficiency of the receiver
$\dot{Q}$	Heat transfer rate [kW]	φ	Maintenance factor
ρ	Reflectance of collector surface	τ	Glass cover transmittance [−]
s	Specific entropy [kJ/kg.°K]	**Subscripts**	
S	Solar radiation absorbed [W/m2]	ch	Chemical
t	Time [h]	cond	Condenser
T	Temperature [°C]	cv	Control volume
T_0	Ambient temperature [°C]	D	Destruction
v	Velocity [m/s]	e	Exit
W	Power or Work [kW]	eva	Evaporator
x	Salinity [ppm]	i	Inlet
Z	Investment cost [USD]	ph	Physical
$\dot{Z}$	Cost rate [USD/h]	pp	Pinch point
		tur	Turbine
		w	Associated with work

1. Introduction

The global energy landscape faces major challenges due to rising demand, which increased by 2.2 % in 2024 [1], nearly twice the decade's average, and the continued reliance on fossil fuels, which met two-thirds of this growth [2]. Fossil fuels still dominate electricity and hydrogen production, supplying about 60 % of global power [3] and nearly 96 % of the hydrogen output [4,5]. This heavy reliance contributes significantly to greenhouse gas emissions [6], which in turn drives environmental degradation [7] and climate change, with serious ecological and public health consequences [8]. Against this backdrop, green hydrogen generated from renewable resources offers a low-carbon pathway for energy transition [9], providing a sustainable alternative that reduces reliance on fossil fuels and greenhouse gas emissions [10], while also serving as a scalable solution aligned with global decarbonization and sustainable development goals [11]. Hydrogen combustion generates water as its sole by-product, offering a zero-carbon alternative to conventional fuel [12,13]. Moreover, when hydrogen is derived from solar-thermal energy, it can be sustainably co-produced with pure oxygen, an arrangement that further supports system-wide decarbonization across multiple sectors [14].

Among the available electrolyzer technologies, Proton Exchange Membrane Electrolyzer (PEMEs) and Anion Exchange Membrane Electrolyzer (AEMEs) have emerged as promising candidates for renewable-driven hydrogen production using water electrolysis. PEMEs are favored for their high current density, rapid dynamic response, and compact design [15], making them suitable for direct coupling with variable renewable sources [16]. Recent studies have demonstrated continuous improvements in PEME durability and efficiency through the use of advanced catalyst layers and membrane materials [17]. AEMEs, on the other hand, offer the advantage of using non-precious metal catalysts and alkaline operation while maintaining relatively high efficiency [18], making them an attractive low-cost alternative for large-scale deployment [19]. Parallel to these developments, recent studies have shown that the advanced scheduling of Alkaline Water Electrolyzers (AWEs) can improve solar utilization above 94 % while reducing operational stress, underscoring their complementary role in renewable-driven hydrogen pathways [20]. Incorporating these electrolyzer advancements into solar-thermal-driven systems is crucial to achieving scalable and cost-effective pathways for green hydrogen production.

While electrolyzer development continues to advance, the efficiency and viability of green hydrogen also depend strongly on the choice of renewable energy resources. Among renewable options, solar-thermal technologies stand out for their scalability, high conversion efficiency, and inherent thermal-storage capability, making them particularly suitable for continuous hydrogen production [21,22]. Several articles indicated that integrating solar-thermal systems with hydrogen production can deliver significant emission reductions and competitive costs in real-world applications such as green ports [23], achieve high efficiencies and lower carbon footprints [24], and provide a sustainable alternative to fossil fuels within broader renewable hydrogen strategies [25]. For instance, a recent study showed that using Parabolic Trough Collectors (PTC) with thermal storage reduced capital cost up to 22.7 % and hydrogen cost by 12.3 % in sunny regions, confirming the financial and ecological benefits of solar-thermal hydrogen generation [26]. Another example highlighted that tailored solar-thermal hydrogen system designs across solar-rich countries like Australia and China can significantly improve productivity and reduce hydrogen costs, confirming the economic viability of location-specific integration strategies [27]. Another study demonstrated that using Concentrating Solar Thermal (CST) systems for thermochemical and solid oxide electrolysis in high solar regions achieved hydrogen production rates above 25 kg/h, with scope to further reduce the Levelized Cost of Hydrogen (LCH) over system optimization [28].

Despite these promising outcomes, a critical gap remains in how integrated solar-thermal hydrogen systems are designed, modeled, and evaluated under realistic operating conditions [22,29]. Most existing studies tend to focus on isolated components or simplified configurations, such as hybrid residential solar–hydrogen systems [30] or solar-driven Steam Methane Reforming (SMR) with thermal storage [31], while overlooking key real-world complexities like fluctuating solar availability, system interactions, and operational scalability. Recent research further shows that climatic variability, including solar radiation intensity, ambient temperature, and seasonal shifts, has a strong impact on system efficiency and viability, whether in large-scale hybrid deployments [32], solar-powered HHO gas production under varying weather [33], or Photovoltaic (PV)–electrolyzer configurations optimized for diverse conditions [34]. Australia exemplifies this dual challenge, offering abundant solar resources [35] but substantial regional and seasonal variability in availability [36]. In response, several studies have begun exploring integrated solar-thermal configurations, such as coupling PTCs with Steam Rankine Cycles (SRC), and PEME [37], extending to cascaded SRC–Organic Rankine Cycle (ORC) systems co-producing hydrogen, oxygen, and hot water [38], or optimizing PTC–Rankine fuel-cell hybrids for scalable hydrogen production [39], highlighting the promise of end-to-end designs. This approach could enable a fully solar-driven hydrogen pathway by combining the high thermal efficiency of PTCs demonstrated in PTC–Thermal Energy Storage (TES)–Kalina–PEM configurations [40] with the operational stability of SRCs and the fast responsiveness of PEMEs, as highlighted in hybrid PTC–PEME–fuel cell systems optimized for efficiency and cost [41]. However, current literature often treats these technologies in isolation; for example, solar thermochemical cycles have been analyzed primarily from the perspective of component design and cost [14], while electrolyzer-based systems such as AE, PEME, and SOEC have been reviewed largely in terms of their standalone thermodynamic and economic performance [42]. As a result, questions about their combined performance and climate adaptability remain unanswered. The present study is the first to comprehensively integrate PTC–SRC–PEME systems with AI-based multi-objective optimization using hourly real-world climatic data, simulating an end-to-end solar-driven system under varied climatic conditions to assess its feasibility, energy efficiency, and climate-responsive viability.

Maximizing the performance of unified solar-thermal hydrogen setups requires careful balancing of conflicting objectives, such as thermal, energy, and exergy efficiency, alongside environmental and economic factors. Prior studies have highlighted optimization trade-offs in hybrid solar–hydrogen systems [30], advanced solar-thermal cycles with electrolysis [43], and broader long-term energy system models [44]. Multi-objective optimization offers a holistic approach to resolve these trade-offs, as shown in hybrid renewable–hydrogen community systems [45], emergy-based integrated energy assessments [46], and hybrid solar-wind-hydrogen networks [47], ensuring viability under varying environmental and operational conditions. Recent studies highlight the effectiveness of Artificial Intelligence (AI) approaches, such as Neural Networks (ANNs) and Genetic Algorithms (GA) in energy research [48]. AI has been shown to optimize renewable integration and enhance energy system resilience [49], improve forecasting, monitoring, and control strategies for renewable energy systems [50], and support multi-objective optimization in advanced solar-driven multi-generation setups [51]. Together, these approaches capture nonlinear system interactions, enabling accurate prediction and optimization of key outputs like energy efficiency and cost. For instance, a hybrid ANN–GA model optimized a solar–geothermal hydrogen system, boosting efficiency to 34.5 % (energy) and 46 % (exergy), while reducing hydrogen cost to 1.49 USD/kg, demonstrating ANN's strength in real-time adaptation and performance prediction [52]. Similarly, ANN combined with Grey Wolf Optimizer enhanced a heliostat–PEME–Compressed Air Energy Storage (CAES) to 47.9 % exergy efficiency and 76.3 MW output in Riyadh's climate, showing ANN's scalability and effectiveness in managing trade-offs in hybrid systems [53]. Another study applied ANN-assisted optimization to a hybrid CAES–SRC–PEME setup, achieving 37.8 % exergy round-trip efficiency with accurate predictions from 2000 simulation datasets, demonstrating ANN's scalability in complex multi-criteria design [54]. In related work, multi-criteria decision-making approaches, such as the Technique for Order Preference by Similarity to Ideal Solution (TOPSIS) have been employed to streamline fluid selection [55] and site selection [56,57], while also balancing thermal properties, safety, cost, and performance in ANN-assisted optimizations of integrated solar–thermal–hydrogen systems [55]. Despite this progress, few studies have applied AI-driven, multi-objective frameworks specifically for PTC–SRC–PEME systems; and the lack of site-specific, fluid-aware strategies continues to hinder scalable, climate-responsive hydrogen solutions.

The current article develops and optimizes a novel solar-driven multi-generation setup that integrates PTC, an SRC, and PEME. Beyond hydrogen, this system enables oxygen and power co-production, enhancing energy utilization and improving economic feasibility. Using ANN for multi-objective optimization and the TOPSIS approach for fluid selection, the system is evaluated under real-world hourly weather data across six Australian cities, Melbourne, Sydney, Canberra, Bunbury, Perth, and Adelaide, moving beyond conventional single-location studies to provide climate-responsive, multi-city siting guidance. Performance is assessed using detailed thermodynamic modeling in Engineering Equation Solver (EES), linking techno-economic outputs with quantified environmental value, including avoided CO_2 and green-space equivalence. The framework positions hydrogen as the principal product while rigorously accounting for oxygen and electricity co-production, capturing synergies often overlooked in earlier research. Overall, this study combines solar thermal (PTC–SRC) and PEM electrolysis within a finance-aware, AI-driven optimization framework that is rarely addressed in prior system-level works, offering novel sustainability insights and contributing to United Nations Sustainable Development Goal 7 [58]. This article is organized as follows: Section 2 covers methodology, Section 3 discusses the results, Section 4 explains limitations and suggests future studies, and Section 5 provides the conclusions.

2. Materials and methods

This study develops and evaluates a solar-driven integrated setup capable of producing liquid hydrogen, oxygen, and electricity simultaneously. The system is modeled thermodynamically, through energy and exergy analysis, and economically, by calculating cost rates. The system was optimized through a hybrid ANN and GA approach aimed at maximizing energy and exergy performance while reducing operational costs. EES software is used for simulation, and key design parameters are informed by validated literature sources. A case study is conducted across six climatically diverse Australian cities, Melbourne, Sydney, Bunbury, Perth, Adelaide, and Canberra, to assess system performance and feasibility. Finally, environmental benefits are evaluated by quantifying carbon emission reductions and potential green space expansion. The overall method is summarized in Fig. 1, with detailed steps presented in Sections 2.1 to 2.5.

2.1. System description

The designed multi-generation configuration integrates a PTC, an SRC, a PEME, and a hydrogen liquefaction subsystem to concurrently generate power, liquid hydrogen, oxygen, and domestic hot water. As shown in Fig. 2, solar irradiation is captured by the PTC and conveyed through a heat transfer fluid to an evaporator, where steam is generated. The steam drives a turbine connected to a generator, producing electricity. After expansion, the steam is condensed and recirculated by two pumps, completing the SRC loop.

A portion of the generated electricity powers the PEME, where water is decomposed into hydrogen and oxygen. Domestic hot water is recovered from the evaporator stage. The generated hydrogen undergoes compression and sequential cooling through a cascade of five heat exchangers and a superheater before being stored in a cryogenic tank as liquid hydrogen. Simultaneously, oxygen is collected in a high-pressure tank, and nitrogen, separated during the cooling stages, is liquefied through parallel heat exchange and stored. This integrated configuration enables efficient resource conversion and storage under varying ambient and solar conditions.

2.2. Thermodynamic modeling

Thermodynamic modelling was carried out in EES under steady-state conditions, with system performance evaluated through mass, energy, and exergy balances following standard formulations reported in the literature [59,60]. To avoid redundancy, general governing equations are not restated here; instead, emphasis is placed on the specific modelling approach, assumptions, and verification applied in this study.

Key modeling assumptions included.

- Turbine and pump processes are treated as isentropic, with efficiencies applied as correction factors.
- Pressure drops in pipelines were assumed to be negligible.
- Evaporator and condenser outlets were specified as saturated conditions.
- Kinetic and potential energy variations were neglected.
- Thermophysical properties of the working fluid were extracted from the EES database using real-fluid correlations.

Each system component (PTC, evaporator, turbine, condenser, and pumps) was modeled using component-specific energy balances, with outputs feeding into the integrated system performance assessment. Exergy destruction in each component was calculated to identify major irreversibility across the cycle. The accuracy of the PEME model was confirmed through validation against literature data (Section 2.4.1, Fig. 6).

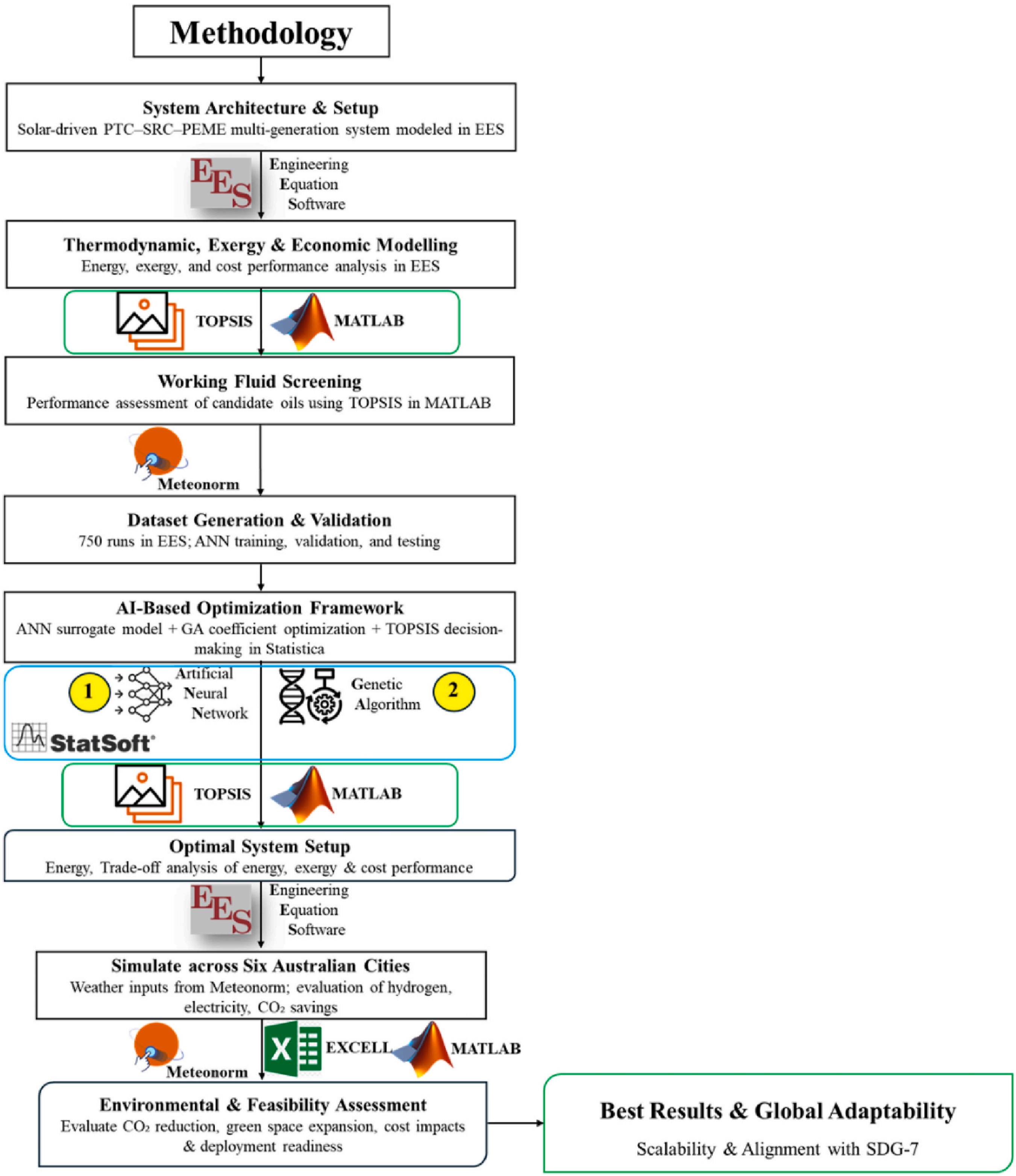

Fig. 1. Methodological Flowchart for system evaluation.

2.2.1. *Component-level energy modeling*

Each system component (turbine, pumps, evaporator, condenser, and PTC) was modeled under steady-state conditions using standard enthalpy-based energy balances. The representative governing equations are summarized in Table 1, which formed the basis of the thermodynamic model implemented in EES. These relations were then coupled with solar collector performance equations and system-level optimization. The net power output was obtained as:

$$\dot{W}_{net} = \dot{W}_{tur} - \dot{W}_{pump1} - \dot{W}_{pump2} \tag{1}$$

2.2.2. *Solar collector modeling*

The thermal behavior of the PTC was modeled using validated solar-thermal performance relations from established literature [61,62]. Key

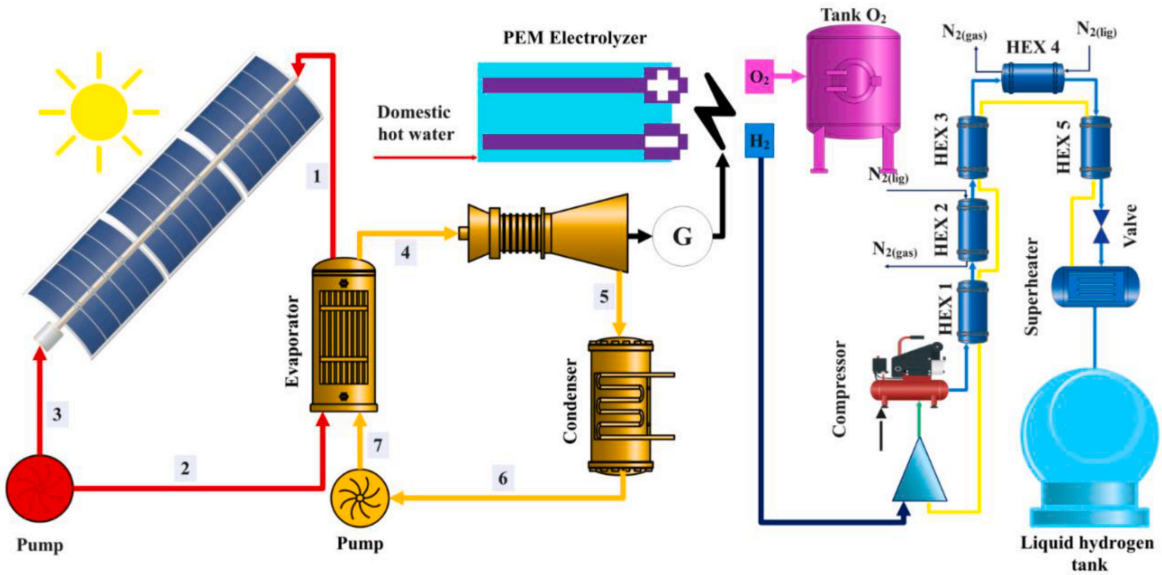

Fig. 2. Integrated solar-based system for electricity, hydrogen, oxygen, and heat generation.

Table 1
Governing energy balance relations applied in component modeling.

System components	Equation
Turbine	$\dot{W}_{tur} = \dot{m}_4 \times (h_4 - h_5)$
Pump No. 1	$\dot{W}_{pump1} = \dot{m}_2 \times (h_3 - h_2)$
Pump No. 2	$\dot{W}_{pump2} = \dot{m}_6 \times (h_7 - h_6)$
Evaporator	$\dot{Q}_{eva} = \dot{m}_7 \times (h_4 - h_7)$
Condenser	$\dot{Q}_{cond} = \dot{m}_5 \times (h_5 - h_6)$
PTC	$\dot{Q}_{(1-2)} = \dot{m}_3 \times (h_1 - h_3)$

These governing relations provided the input conditions for solar collector modeling described in Section 2.2.2.

parameters were set as: glass cover transmittance ($\tau = 0.96$) for glass cover transmittance, $k = 16$ W/m°K for receiver conductivity, and $U_l = 3.82$ W/m$^{2\circ}$K for the heat loss coefficient.

Collector performance was primarily evaluated through the useful heat gain and heat removal factor (Equations (2) and (3)), which quantify the effective thermal capture and transfer to the working fluid. The collector area required to meet the system's energy demand was then calculated from the useful heat balance (Equation (4)).

$$\dot{Q}_u = n_{ptc} F_R \times \left[S A_{ap} - A_r \times U_l \times (T_3 - T_0)\right] \tag{2}$$

$$F_R = \frac{\dot{m}_C \times C_{P_c}}{A_r \times U_l}\left[1 - \exp\left(\frac{A_r \times U_l \times F_l}{\dot{m}_C \times C_{P_c}}\right)\right] \tag{3}$$

$$A_p = n_{ptc} + A_{ap} \tag{4}$$

Here, S, represents the absorbed solar radiation per unit area, which depends on the incident solar irradiance and the collector's optical efficiency (η_r). The latter is determined by the reflectivity, transmissivity, and absorptivity of the optical elements [63]. The overall thermal resistance of the absorber tube (F_1) was also considered, but follows standard formulations available in the literature [61,62] and is not restated here for brevity.

Collector performance parameters were then combined with design and boundary conditions (Section 2.2.3)

2.2.3. *Design parameters*

The environmental and design input variables applied in the thermodynamic modeling are listed in Table 2, considering validated literature sources [64,65].

Table 2
Environmental and design input parameters for thermodynamic modeling.

Parameter	Parameter Definition	Unit	Amount
Environmental Parameters			
T_0	Ambient temperature	°C	25
P_0	Ambient pressure	kPa	101.3
T_{sun}	Solar temperature	°C	5800
G_b	Solar radiation intensity	W/m^2	850
Thermodynamic Components			
T_1	Evaporator inlet temperature	°C	360
$\dot{m}_1$	Evaporator mass flow rate	kg/s	10
pp_{Eva}	Evaporator pinch point	°C	5
P_1	Evaporator inlet pressure	kPa	250
P_4	Turbine inlet pressure	kPa	1500
η_{Pump}	Pump efficiency	%	90
P_7	Pump inlet pressure	kPa	100
pp_{Cond}	Condenser pinch point	°C	5
U_l	Collector heat loss coefficient	W/m$^{2\circ}$C	3.82
K	Receiver thermal conductivity coefficient	W/m$^{2\circ}$C	16
τ	Glass cover transmission coefficient	–	0.96

2.2.4. *Proton Exchange Membrane Electrolyzer (PEME) and exergy analysis*

All net electrical output of the system was directed to the PEME to prioritize hydrogen generation:

$$\dot{W}_{PEM} = \dot{W}_{net} \tag{5}$$

The PEME subsystem was modeled under standard operating conditions representative of commercial-scale units. Hydrogen production was determined using an empirically validated polynomial correlation (Eq. (6)), with coefficients obtained through regression of experimental polarization data reported by Ref. [66]. The boundary conditions and technical parameters applied are summarized in Table 3, consistent with

Table 3
PEME model boundary conditions and parameters [66].

Parameter	Unit	Value
Operating temperature	°C	80
P_0	kPa	101.3
Current density range	A/m^2	0–6000
Cell potential range	V	1.57–1.82
Membrane thickness	μm	180

the validation benchmark (Section 2.4.1, Fig. 6)

$$\dot{M}_{H2_{Out}}(\dot{m}_{24}) = \alpha_{H2} \times \dot{W}_{PEM}{}^{b_{H2}} + C_{H2} \rightarrow \begin{cases} \alpha_{H2} = 3.382 \times 10^{-6} \\ b_{H2} = 0.9727 \\ C_{H2} = 5.928 \times 10^{-6} \end{cases} \tag{6}$$

This correlation accounts for the nonlinear relationship between electrical input and hydrogen output and has been validated in prior studies [67,68].

Exergy analysis was also conducted to identify the main sources of irreversibility in the integrated cycle. Both physical and chemical exergy were considered, following standard formulations reported in the literature [69,70]. Exergy destruction for each component was then obtained from the difference between input and output exergy, enabling quantification of major efficiency bottlenecks.

2.3. Climate and location data

Fig. 3 presents the Global Horizontal Irradiation (GHI) map of Australia, highlighting the continent's strong solar potential. To evaluate the proposed integrated solar-driven system, six representative cities, Melbourne, Sydney, Bunbury, Perth, Adelaide, and Canberra, were selected as case study sites. These locations span temperate, Mediterranean, and semi-arid zones, providing a comprehensive basis for assessing technical, thermodynamic, and economic performance under varied climatic conditions.

Although northern regions, such as Darwin and Alice Springs, and Brisbane on the East Coast, exhibit the highest GHI values, the six chosen cities were prioritized for their relevance to potential deployment. Selection was guided by four main criteria.

- **Urban demand and infrastructure readiness:** all selected cities are metropolitan hubs with developed energy grids and significant population density;
- **Climatic representativeness:** sites capture variability in solar resource intensity, seasonal temperature ranges, and humidity profiles;
- **Policy alignment:** these cities are centers of active renewable energy initiatives and regulatory support;
- **Deployment feasibility:** accessibility to research institutions, industry partners, and logistical networks enhances the potential for pilot-scale demonstrations.

It should be mentioned that Brisbane was not included to avoid redundancy with Sydney, which already represents the east coast's humid subtropical climate, ensuring broader climatic diversity across the selected case studies.

For each city, site-specific hourly meteorological data, including ambient temperature, solar irradiance, and atmospheric pressure, were obtained using the Meteonorm 8.0 database [72], which interpolates long-term weather records to generate consistent datasets for simulation. These data ensured reliable and standardized model inputs for evaluating the PTC–SRC–PEME system under diverse climatic conditions.

Hourly weather files from Meteonorm 8.0 were generated and summarized to monthly averages for presentation. Fig. 4 summarizes mean ambient temperature profiles across the six cities; values span roughly 0 °C–25 °C, with peaks in December–February (austral summer). For comparison, the annual mean ambient temperatures are approximately 18.25 °C in Melbourne and 18.03 °C in Bunbury, highlighting the relative climatic similarity of these cities despite seasonal fluctuations. From a system performance perspective, these variations are critical because higher summer temperatures align with stronger solar input but reduce thermal gradients in the cycle, whereas cooler winter conditions improve cycle efficiency but coincide with lower solar availability. This interplay highlights the importance of site-specific climate data in evaluating the feasibility and performance of the integrated PTC–SRC–PEME system.

Fig. 5 presents the monthly average GHI across the six case study cities. Values peak during the austral summer months (December–February), with Perth, Bunbury, and Adelaide showing the highest irradiance levels, while Melbourne, Sydney, and Canberra record comparatively lower values. Seasonal variability is pronounced, with irradiance dropping significantly during the winter months

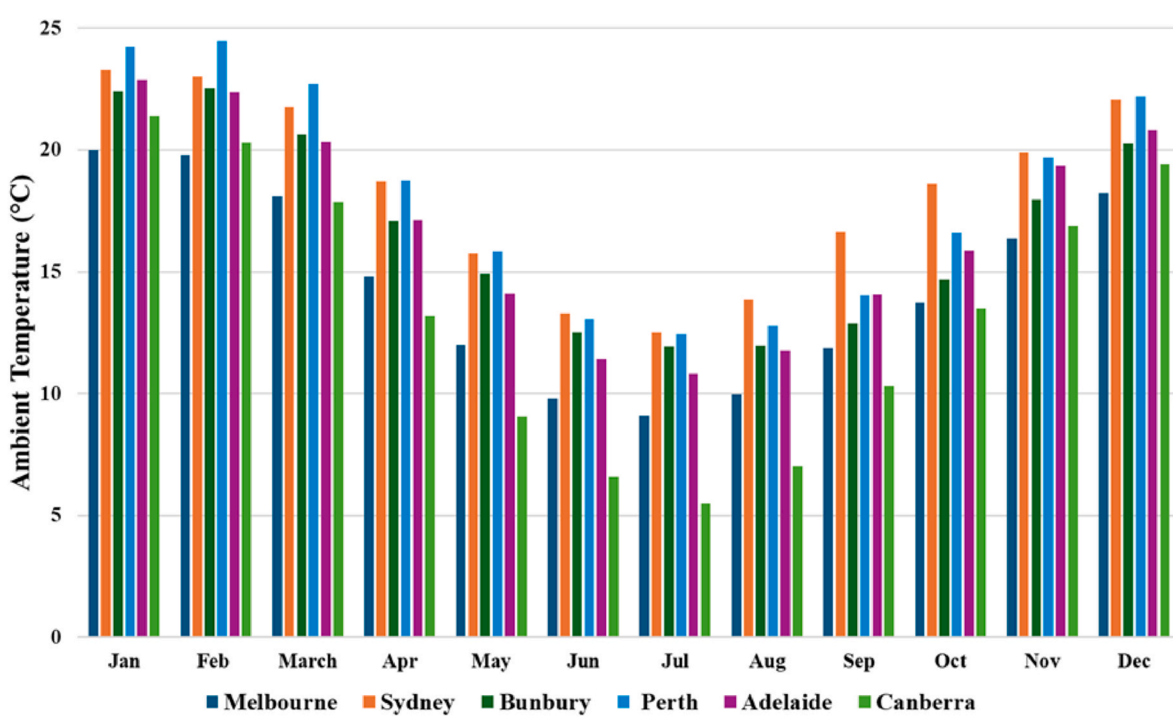

Fig. 3. Solar map of Australia [71].

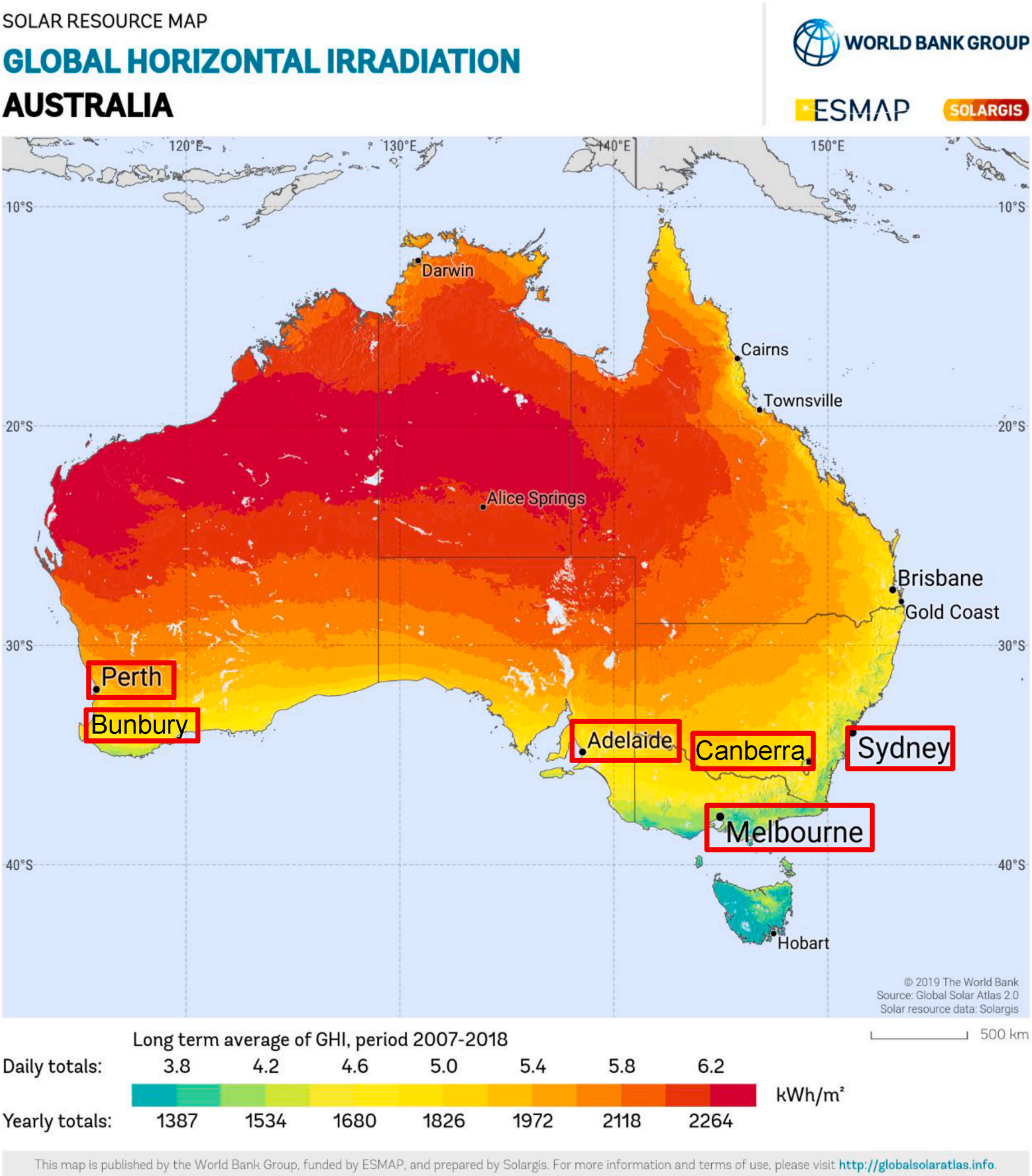

Fig. 4. Monthly average ambient temperature for the six selected Australian cities [72].

(June–August). These trends are crucial for evaluating the PTC–SRC–PEME system, as higher irradiance directly increases thermal input to the collector, thereby enhancing the potential for hydrogen and electricity generation. In contrast, lower winter irradiance highlights the importance of system optimization for year-round feasibility.

2.4. Optimization methodology

To evaluate and optimize the performance of the recommended PTC–SRC–PEME setup, a structured three-step optimization framework was developed in Statistica. First, a comprehensive dataset was created by performing approximately 750 simulation runs EES. In each run, seven key decision variables were varied within realistic engineering ranges: (i) number of parabolic collectors, (ii) evaporator inlet

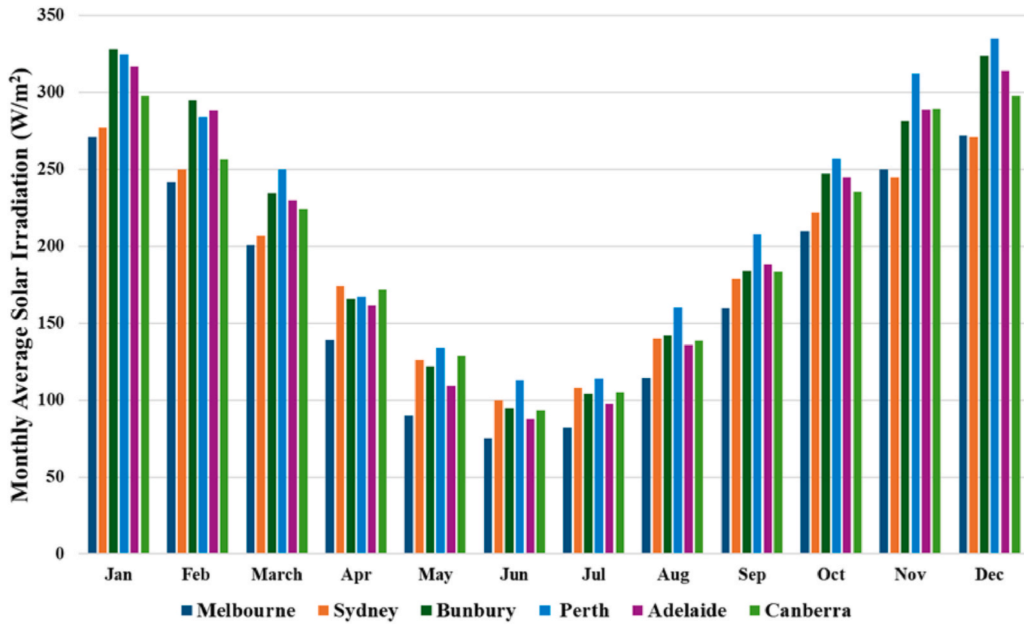

Fig. 5. Monthly average solar irradiance (GHI) for the six selected Australian cities [72].

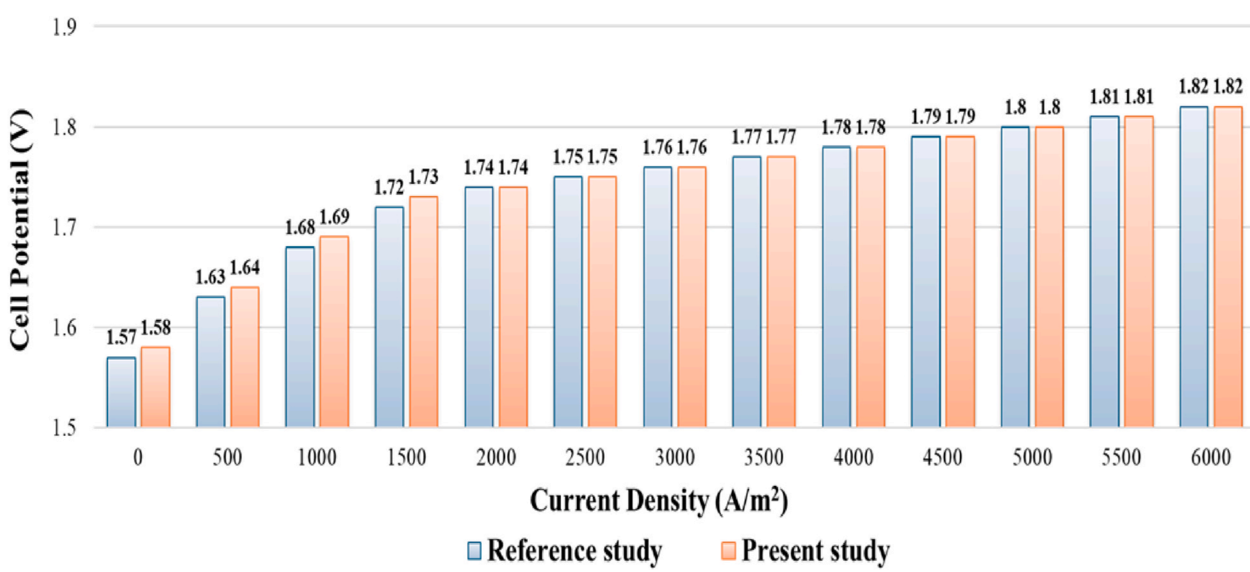

Fig. 6. Validation of PEME subsystem against experimental data [66].

temperature, (iii) steam turbine inlet pressure, (iv) steam pump inlet pressure, (v) evaporator pinch point temperature, (vi) turbine efficiency, and (vii) pump efficiency. Each simulation produced outputs for energy efficiency, exergy efficiency, and cost rate, thereby creating a rich dataset of input–output relationships. To avoid overfitting and ensure generalization, the dataset was split into training, validation, and testing groups.

In the second step, this dataset was used to develop a predictive ANN model in Statistica. The ANN was trained to capture nonlinear interactions among seven input parameters and three output indicators. Following training and validation, the ANN served as a fast and reliable surrogate model for the detailed thermodynamic simulations. The ANN was then coupled with a GA in Statistica, which iteratively explored the design space to identify configurations that maximized performance (energy and exergy efficiency) at a lower cost rate. The GA produced a Pareto front of non-dominated solutions, reflecting trade-offs among competing objectives and ensuring that optimal designs were not limited to a single criterion.

Finally, the third step applied TOPSIS to the GA-derived solutions in MATLAB. In this step, the objective functions were normalized and weighed equally to avoid bias. TOPSIS was applied to evaluate the relative proximity of each alternative to the ideal and anti-ideal points. The option with the greatest closeness value was identified as the optimal configuration, reflecting the best compromise among technical efficiency, thermodynamic performance, and economic feasibility.

2.4.1. Validation

The PEME subsystem represents the most complex and non-linear component of the proposed system, making its validation essential for ensuring reliable simulation outcomes. Consistent with common practice in energy systems modeling [73], validation was performed by comparing the EES-based model against experimental polarization data from the literature [66]. As illustrated in Fig. 6, the predicted cell potential–current density profile closely matches the experimental results, confirming that the thermodynamic model accurately captured the nonlinear electrochemical behavior of the PEME. This agreement establishes confidence in the modeling assumptions and ensures that the simulation outputs are both realistic and representative for subsequent optimization and system-wide performance assessments.

2.4.2. TOPSIS-based fluid selection

Heat transfer fluid choice significantly affects PTC thermal behavior. Four candidate oils, Syltherm 800, Marlotherm SH, Therminol VP1, and Therminol 59, were evaluated under identical conditions. Key indicators included production rate, energy and exergy efficiency, and cost rate. To identify the most suitable fluid, the TOPSIS method was applied in MATLAB (R2022a) [74]. TOPSIS was selected because it offers a transparent and computationally efficient approach to rank alternatives based on their distance to ideal solutions, making it particularly suitable for balancing competing technical and economic criteria. Unlike methods such as the Analytic Hierarchy Process (AHP), which relies on subjective pairwise comparisons, or Elimination and Choice Expressing Reality (ELECTRE), which applies complex outranking rules, TOPSIS provides a direct and reproducible ranking framework that aligns with the goals of this study. The process involved constructing a decision matrix, normalizing performance values, and calculating each option's closeness to the ideal and non-ideal references. To ensure fairness, exergy efficiency and cost rate were given equal weight, balancing technical and economic priorities. Detailed performance results for the candidate fluids and their TOPSIS ranking are presented in the Results section.

2.5. Economic and environmental analysis

For economic analysis, component cost rates were evaluated following standard engineering economics relations [75]. Investment cost, maintenance factor, and the Capital Recovery Factor (CRF) were considered to annualize costs over the system lifetime. Table 4 summarizes the cost balance relationships for the main subsystems, including the turbine, condenser, evaporator, pumps, PTC field, and recuperators. By aggregating the cost rates of individual components, the cost rate of the whole setting was obtained and used as an objective in the multi-objective optimization. This approach ensured that the economic feasibility was evaluated alongside energy and exergy efficiency.

The environmental analysis was conducted to quantify the system's decarbonization potential. Carbon dioxide reduction was estimated by comparing the hydrogen produced from the proposed system with that produced via SMR, the predominant industrial process [76]. The avoided CO_2 emissions were calculated as:

$$\Delta CO_2 = m_{H_2} \times EF_{SMR} \tag{7}$$

where m_{H_2} the annual hydrogen mass output and EF_{SMR} is the emission factor for SMR-based hydrogen production (kg CO_2 per kg H_2). Additional environmental benefits were attributed to the electricity co-produced by the system, which offsets grid-based power from fossil fuels.

To further contextualize these benefits, the avoided CO_2 emissions were expressed as equivalent green space expansion, calculated as the number of trees or hectares of forest required to absorb the same annual CO_2. This provides a tangible sustainability metric aligned with climate policy and urban greening initiatives.

Table 4
Environmental and design input parameters for thermodynamic modeling.

System components	Equation
Turbine	$Z_{Tur} = 4750 \times \left(\dot{W}_{turbine}{}^{0.75}\right) + 60 \times \left(\dot{W}_{turbine}{}^{0.95}\right)$
Condenser	$Z_{Cond} = 1773 \times \dot{m}_5$
Evaporator	$Z_{Eva} = 276 \times \left(A_{Evap}{}^{0.88}\right)$
Pump No. 1	$Z_{Pump1} = 3500 \times \left(\dot{W}_{Pump1}{}^{0.41}\right)$
Pump No. 2	$Z_{Pump2} = 3500 \times \left(\dot{W}_{Pump2}{}^{0.41}\right)$
PTC	$Z_{PTC} = 240 \times A_P$
REC1	$Z_{REC1} = 12000 \times \left(\left(\frac{A_{REC1}}{100}\right)^{0.6}\right) \times \dot{Z}$
REC2	$Z_{REC2} = 12000 \times \left(\left(\frac{A_{REC2}}{100}\right)^{0.6}\right) \times \dot{Z}$
Separator	$Z_{Separator} = 12000 \times \left(\left(\frac{A_{Separator}}{100}\right)^{0.6}\right) \times \dot{Z}$

3. Results and discussion

This section describes the main results of the proposed solar-driven PTC–SRC–PEME system, combining thermodynamic, economic, and optimization-based analyses. Results are structured to first address subsystem-level design choices, such as working fluid selection, and then move toward whole-system optimization, techno-economic performance, and exergy losses. Seasonal and location-specific assessments across six Australian cities are also reported, followed by environmental co-benefits, deployment prioritization, scalability, and comparative benchmarking with prior studies.

3.1. Working fluid selection for PTC via TOPSIS

The performance of four candidate heat transfer oils, Syltherm 800, Marlotherm SH, Therminol VP1, and Therminol 59, was evaluated for the PTC subsystem output performance, energy and exergy efficiency, and cost rate (Table 5). Syltherm 800 achieved the highest production capacity and efficiency values, while Marlotherm SH offered a slightly lower cost rate. Therminol VP1 and Syltherm 800 demonstrated comparable technical performance, whereas Therminol 59 ranked marginally lower across the indicators.

To identify appropriate fluid, the TOPSIS method was applied, assigning equal weight to efficiency and cost to balance thermodynamic and financial performance. Based on the relative closeness coefficients, Therminol VP1 was selected as the optimal working fluid as shown in Table 6. This choice ensures a favorable compromise between stability, efficiency, and operating cost, reinforcing the contribution of the solar subsystem to the integrated PTC–SRC–PEME configuration.

This outcome aligns with recent studies on working fluid selection in PTC systems. For instance, Therminol VP-1 was shown to outperform water in terms of heat transfer efficiency, thermal stress resistance, and overall thermal performance under typical operating temperatures, while molten salt performed better at higher temperature ranges [77]. Similarly, comparative analyses involving Syltherm 800, Therminol VP-1, and Dowtherm Q found that Therminol VP-1 delivered superior thermal efficiency and operated effectively over a range of design conditions [78].

3.2. ANN–GA optimization framework and outcomes

The ANN–GA framework, implemented in Statistica [79], was employed to assess the effect of seven decision parameters, involving evaporator inlet temperature, turbine and pump efficiencies, and the number of PTC units, on overall system performance (Table 7). A

Table 5
Performance of candidate working fluids for the PTC subsystem.

Collector oil type	Production Capacity (kWh)	Energy Efficiency (%)	Exergy Efficiency (%)	Cost rate (USD/h)
Syltherm_800	606.8	31.32	27.31	49.43
Marlotherm SH	559.4	30.59	26.35	48.8
Therminol_VP1	594.7	31.03	26.99	49.07
Therminol_59	590.4	30.94	26.97	49.21

Table 6
Optimal working fluid for the PTC identified via TOPSIS.

Collector oil type	Production capacity (kWh)	Energy efficiency (%)	Exergy efficiency (%)	Cost rate (USD/h)
Therminol_VP1	594.7	31.03	26.99	35.07

Table 7
Decision parameters and operating ranges for ANN–GA optimization.

Parameter	Unit	Lower limit	Upper limit
Condenser outlet temperature (T1)	°C	5	20
Turbine inlet pressure (P4)	kPa	1300	1800
Pump inlet pressure (P5)	kPa	80	120
Number of parabolic trough collectors	–	85	100
Pinch Point evaporator	°C	3	58
Turbine efficiency	%	75	95
Pump efficiency	%	75	95

surrogate ANN model, trained on 750 EES simulations, enabled rapid assessment of system responses across the multidimensional design space. The GA was then used to optimize these variables, producing the ranges and optimal values summarized in Tables 8 and 9. Results indicated that turbine inlet pressure and evaporator temperature had the greatest impact on energy and exergy efficiency, while pump efficiency and evaporator pinch point played minor roles.

The results highlight that turbine inlet pressure and evaporator temperature had the highest effect on performance, whereas pump efficiency and evaporator pinch point contributed marginally. The Pareto fronts (Fig. 7a–c) demonstrate clear trade-offs: gains in energy and exergy efficiencies generally came with higher cost rates, whereas cost reduction required compromises in technical performance. The near-linear correlations across the plots emphasize the close link between efficiency improvements and cost escalation, emphasizing the need to balance objectives rather than maximize a single one. Specifically, Fig. 7a indicates that energy efficiency increased with cost rate, Fig. 7b confirms the interdependence of energy and exergy efficiencies, and Fig. 7c shows that higher exergy efficiency also raised costs, reinforcing the economic–thermodynamic trade-off.

The distribution profiles of the objective functions (Fig. 8a–c) show that feasible operating conditions cluster around intermediate values, rather than the extremes of maximum efficiency or minimum cost. Energy efficiency (Fig. 8a) and exergy efficiency (Fig. 8b) follow near-normal distributions, with most solutions concentrated around 30–31 % and 26–27 %, indicating stable and realistic efficiency levels for the PTC–SRC–PEME system. In contrast, the cost rate distribution (Fig. 8c) is broader, ranging from about 41 to 53 USD/h, reflecting greater variability in economic performance as technical parameters are adjusted. These distributions show that most feasible operating points cluster around intermediate values of efficiency and cost, indicating that

Table 8
Optimal decision variable values obtained from ANN–GA optimization.

Decision Variable	Unit	Valid N	Mean	Minimum	Maximum
Condenser outlet temperature (T1)	°C	500	370.000	320.000	420.000
Turbine inlet pressure (P4)	kPa	500	1523.000	1200.000	1800.000
Pump inlet pressure (P5)	kPa	500	99.000	80.000	120.000
Number of parabolic trough collectors	–	500	87.000	80.000	95.000
Pinch Point evaporator	°C	500	5.500	3.000	8.000
Turbine efficiency	%	500	0.875	0.700	0.950
Pump efficiency	%	500	0.825	0.700	0.950

Table 9
Optimal values of objective functions from ANN–GA optimization.

Decision Variable	Unit	Valid N	Mean	Minimum	Maximum
Energy efficiency	%	500	30.83662	28.19000	33.50000
Exergy efficiency	%	500	26.32174	24.69000	28.12000
Cost rate	USD/h	500	47.02042	41.33000	53.17000

extremely high-efficiency or low-cost scenarios are less stable and less frequent. This highlights the value of multi-objective optimization in identifying balanced, repeatable operating conditions that align with the practical constraints of solar-driven hydrogen systems.

These findings are consistent with earlier applications of ANN–GA optimization in hybrid energy systems, where nonlinear interactions between thermodynamic and economic parameters required surrogate-assisted exploration of large solution spaces. Studies on optimizing a solar and geothermal–based multi-energy and hydrogen generation setup using an ANN–GA framework indicate improvements in thermodynamic and economic performance across competing objectives [52]. Similarly, another study applied an ANN–GA optimization in a hybrid solar- and biomass-based system (heliostat–PEME), achieving balanced increases in exergy efficiency and reductions in cost [80]. Such findings validate the suitability of ANN–GA in navigating nonlinear trade-offs between efficiency and cost in solar-driven hydrogen system designs.

While the GA produced a set of Pareto-optimal solutions, selecting a single configuration required a systematic decision-making approach to balance competing objectives. To address this, the TOPSIS method was implemented in MATLAB (R2022a) [74] and applied to the GA-derived dataset. Performance indicators were normalized and evaluated relative to ideal and anti-ideal solutions. Equal weighting was assigned to exergy efficiency and cost rate to avoid bias toward purely technical or purely economic preferences.

The TOPSIS procedure selected a configuration yielding 30.83 % energy efficiency, 26.32 % exergy efficiency, and a cost rate of 47.02 USD/h as the optimal compromise solution. This outcome highlights the importance of multi-criteria approaches strengthen optimization robustness, ensuring the selected design avoids extremes such as high-cost or high-efficiency-only outcomes. Integrating ANN–GA optimization with TOPSIS not only improved the transparency of the selection process but also aligned with best practices in multi-generation energy system research. Similar hybrid frameworks reported in solar–hydrogen and CAES–SRC–PEME systems [81] demonstrate that combining surrogate-based optimization with multi-criteria ranking provides context-sensitive, technically sound, and economically viable system designs under real climatic conditions.

3.3. Techno-economic and exergy performance

This section examines the economic distribution of costs across the optimized PTC–SRC–PEME system and identifies the main thermodynamic losses. Fig. 9 shows the cost rate at 47.78 USD/h, dominated by the solar unit (38.17 USD/h), while the PEM-based hydrogen production unit contributed a much smaller share (9.61 USD/h). This result confirms that the solar system is the most cost-intensive element, reflecting the capital- and operation-heavy nature of large parabolic trough fields, and highlighting the importance of targeting collector efficiency improvements to reduce overall system expenditure.

Fig. 10 presents the exergy destruction profile, where the solar field again emerged as the largest contributor, with a cumulative destruction of 3364 kWh, or about 38.66 kWh per collector. The PEM electrolyzer followed with 564 kWh, while the condenser (412 kWh), evaporator (1053 kWh), and steam turbine (194 kWh) also showed notable irreversibility. Pumps contributed negligibly at 1 kWh. In total, the system generated 575 kWh of useful output but incurred 4503 kWh of exergy destruction, highlighting the dominance of solar and electrolysis units in both cost and performance losses. These findings align with recent

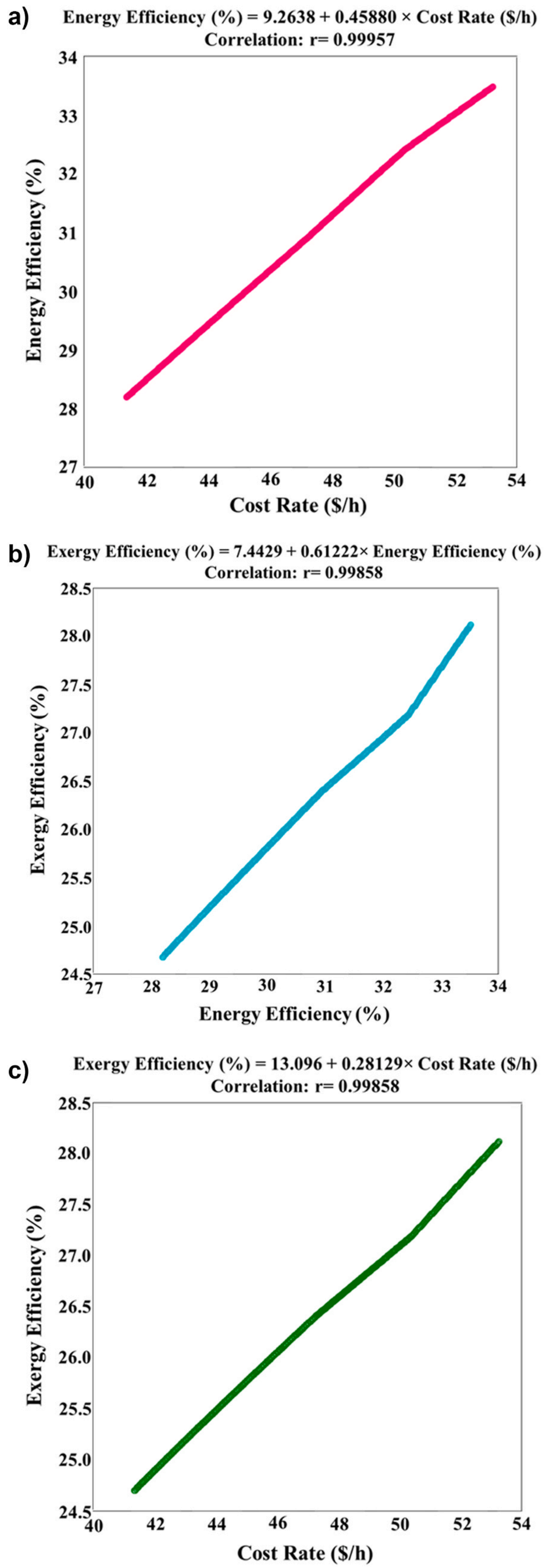

Fig. 7. Pareto fronts (a) energy efficiency and cost rate, (b) exergy efficiency and energy efficiency, (c) exergy efficiency and cost rate.

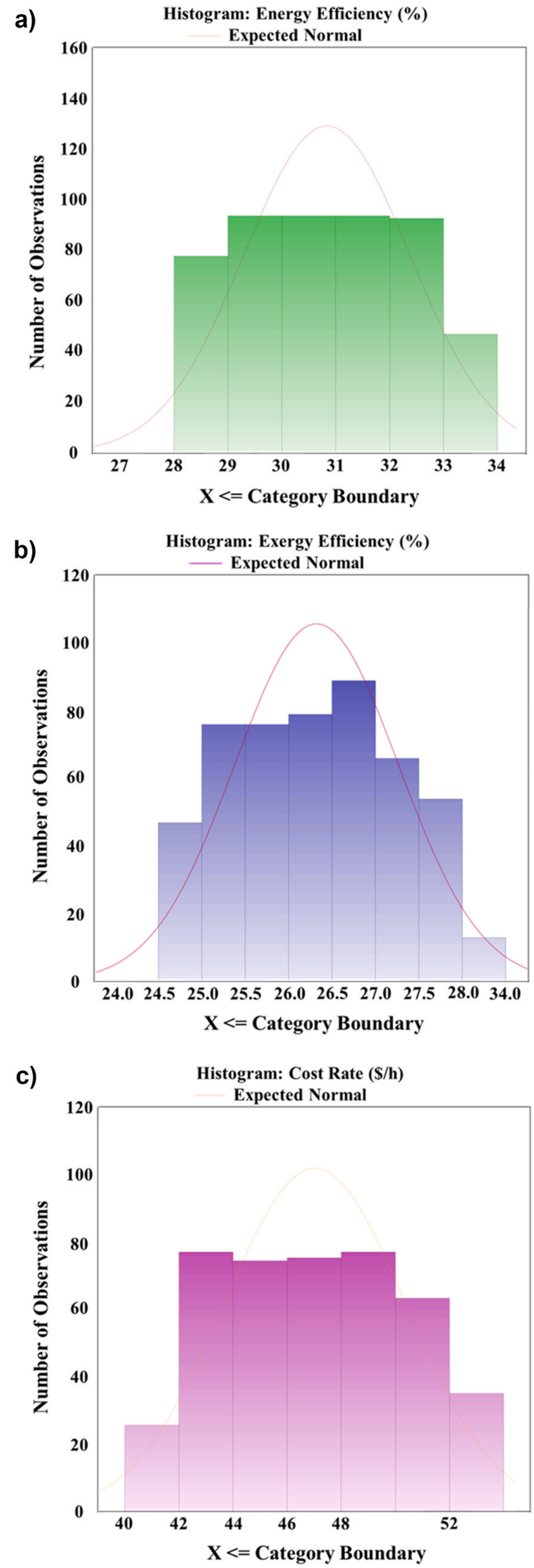

Fig. 8. Distribution of objective functions from ANN–GA optimization.

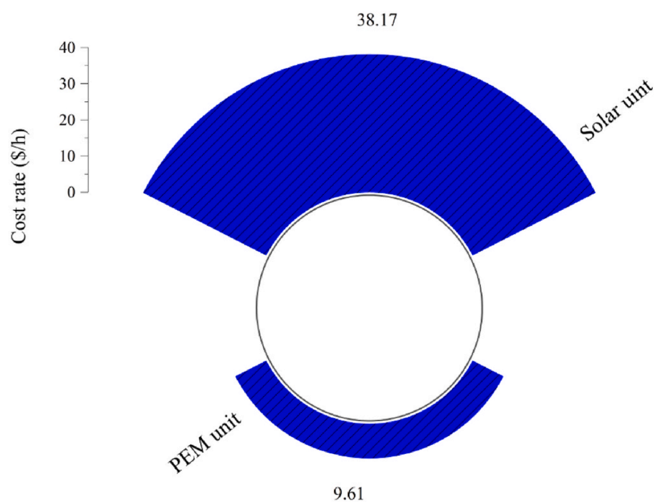

Fig. 9. Cost rate distribution of solar and hydrogen production units.

exergy analysis of integrated solar power systems that showed the PTC subsystem contributes over 85 % of total exergy destruction [82]. Similarly, another study indicated that solar collectors often dominate irreversibility in solar-based cycles due to high-temperature gradients [83]. Such agreement with earlier studies reinforces the need for technical enhancements focused on solar field efficiency and improved exergy management to bolster both economic and thermodynamic performance in solar-driven hydrogen systems.

3.4. Location-specific performance and environmental benefits

This section presents an inclusive assessment of the proposed solar-driven system across six Australian cities, focusing first on its location-specific performance in terms of power generation, hydrogen and oxygen output, storage capacity, efficiency, and costs, followed by its environmental benefits expressed through avoided emissions, cost savings, and ecological offsets.

3.4.1. Location-specific performance

The technical performance of the system varies according to local solar resource availability, with seasonal and geographic differences shaping energy outputs and hydrogen production potential. Fig. 11 illustrates monthly variations in power output across the six study locations, highlighting strong seasonality driven by solar radiation availability. Higher outputs were recorded during summer months (December to February), especially in Perth, Bunbury, and Adelaide, where higher solar irradiance boosted system performance. In contrast, winter months (June to August) showed reduced power generation across all cities, reflecting the direct dependence of the system on solar input. These seasonal shifts directly influenced hydrogen yields, as shown in Fig. 12, where monthly production consistently peaked in summer (December–February) and declined in winter (June–August). This behavior reflects higher solar irradiance and improved thermal capture by the PTC field during the warmer months, which increases steam generation, turbine output, and thus the electricity available to the PEM electrolyzer. Similar seasonal variations in hydrogen production have been observed in recent solar PV-based studies, reinforcing the importance of aligning system deployment with local climate dynamics to sustain year-round performance [84].

Building on this, Fig. 13 shows the seasonal dynamics of liquid hydrogen storage, which closely followed the trends of power and hydrogen output. Storage volumes peaked in summer across all cities, driven by excess hydrogen availability from higher irradiance and conversion efficiency, while winter months saw notable declines due to reduced solar input. Canberra and Adelaide exhibited particularly high seasonal contrasts, pointing out their sensitivity to radiation variability. This finding highlights that storage capacity plays a crucial role in balancing seasonal mismatches between supply and demand, ensuring system resilience. It also confirms that solar-rich months offer

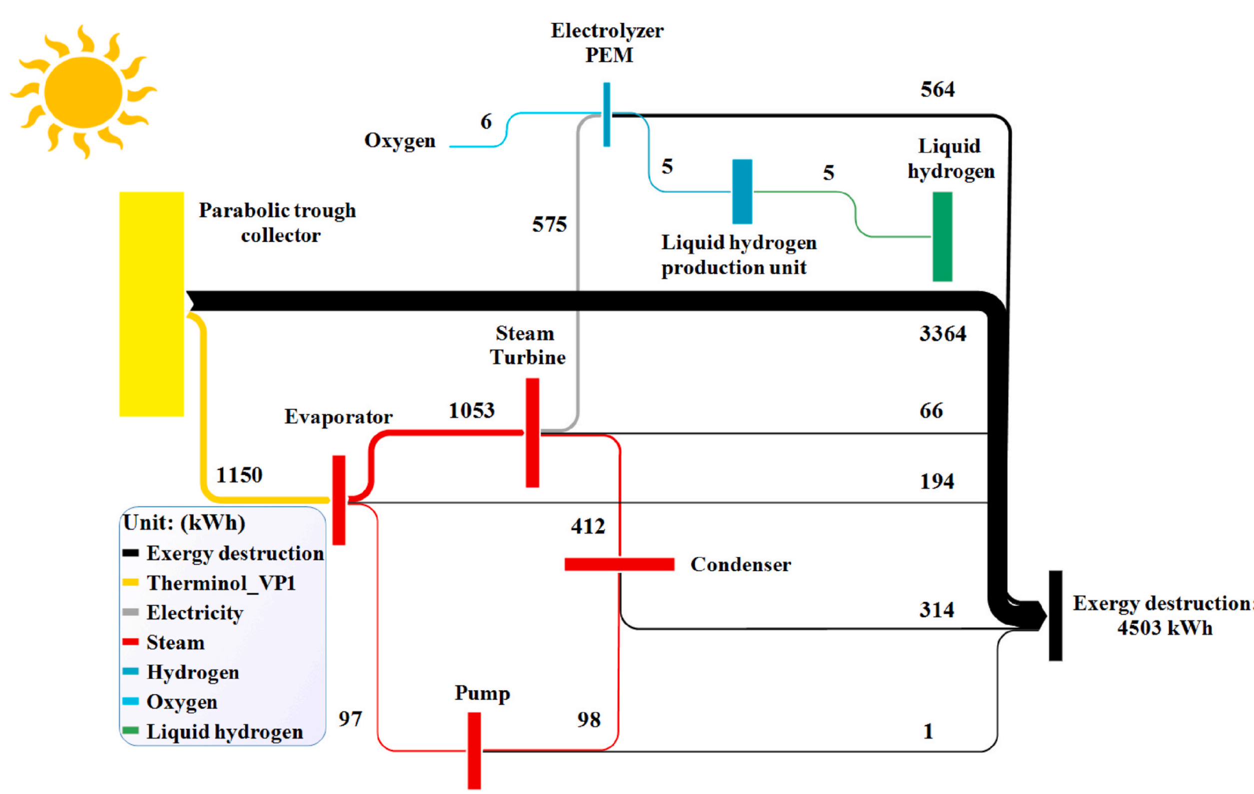

Fig. 10. Exergy destruction across system components.

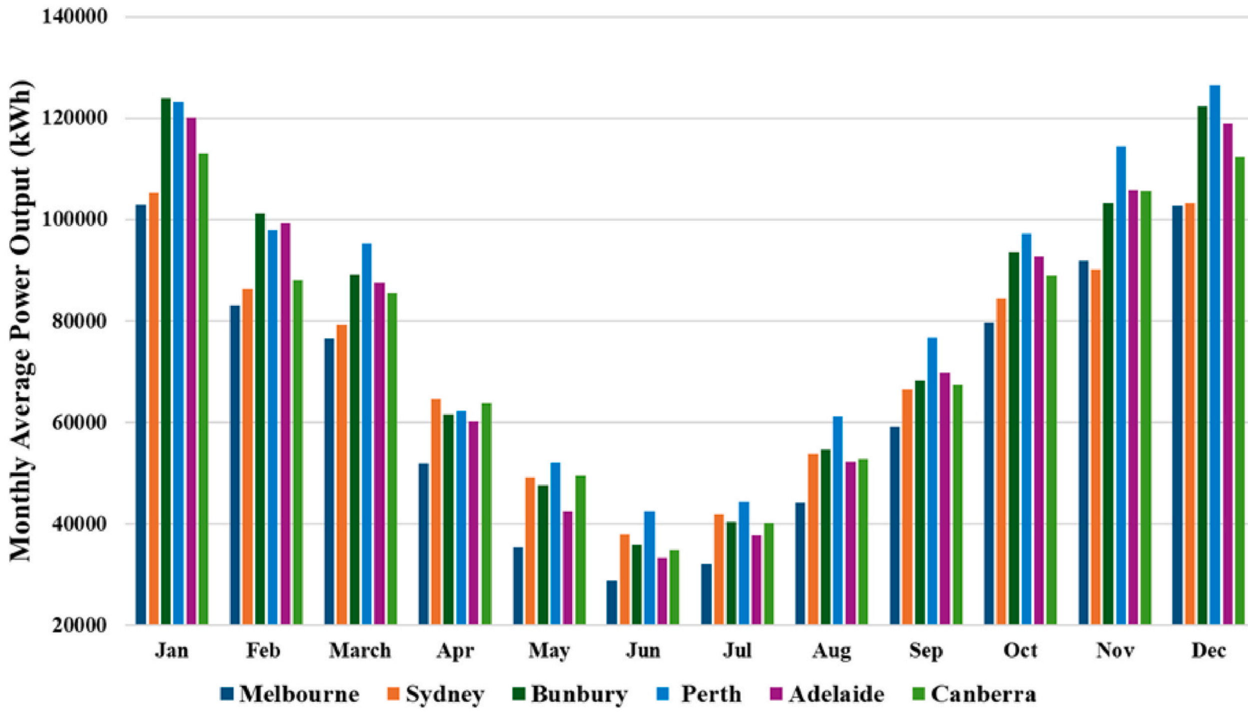

Fig. 11. Monthly power output across six selected Australian cities.

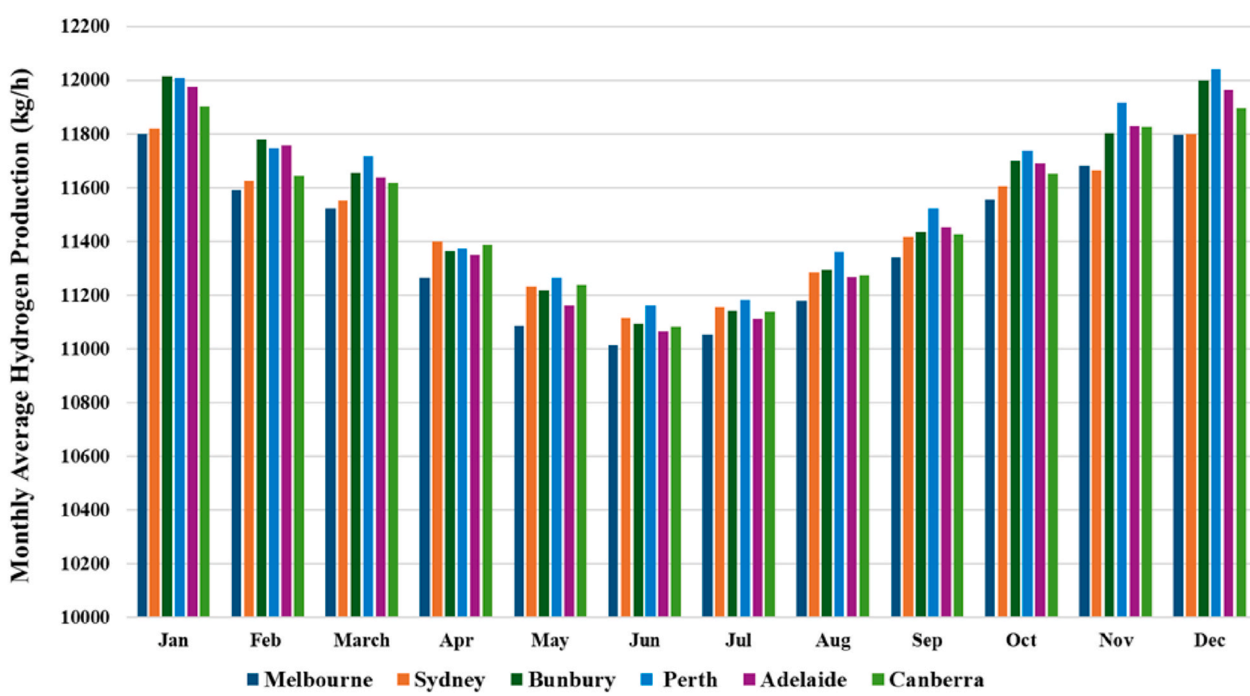

Fig. 12. Monthly hydrogen production across six selected Australian cities.

opportunities to maximize hydrogen liquefaction and build reserves for winter shortages, a strategy emphasized in recent studies on solar-hydrogen integration with storage systems [85].

In parallel, Fig. 14 presents oxygen production across the study cities, which followed a similar seasonal trend to hydrogen output. Oxygen generation increased during summer months due to higher electricity availability from the steam turbine and decreased during winter when solar input was limited. Although variations across cities were relatively smaller compared to liquid hydrogen storage, production in Perth and Bunbury was consistently higher, reflecting their stronger solar resource base. This reinforces the system's co-benefits by simultaneously providing both hydrogen and oxygen, supporting wider industrial applications while enhancing economic feasibility. Such integrated oxygen–hydrogen production aligns with recent analyses of multi-output solar-driven electrolyzer systems, which highlight oxygen as an often-overlooked but valuable by-product that improves overall system sustainability and revenue potential [86].

Figs. 15 and 16 show the seasonal changes of exergy efficiency and

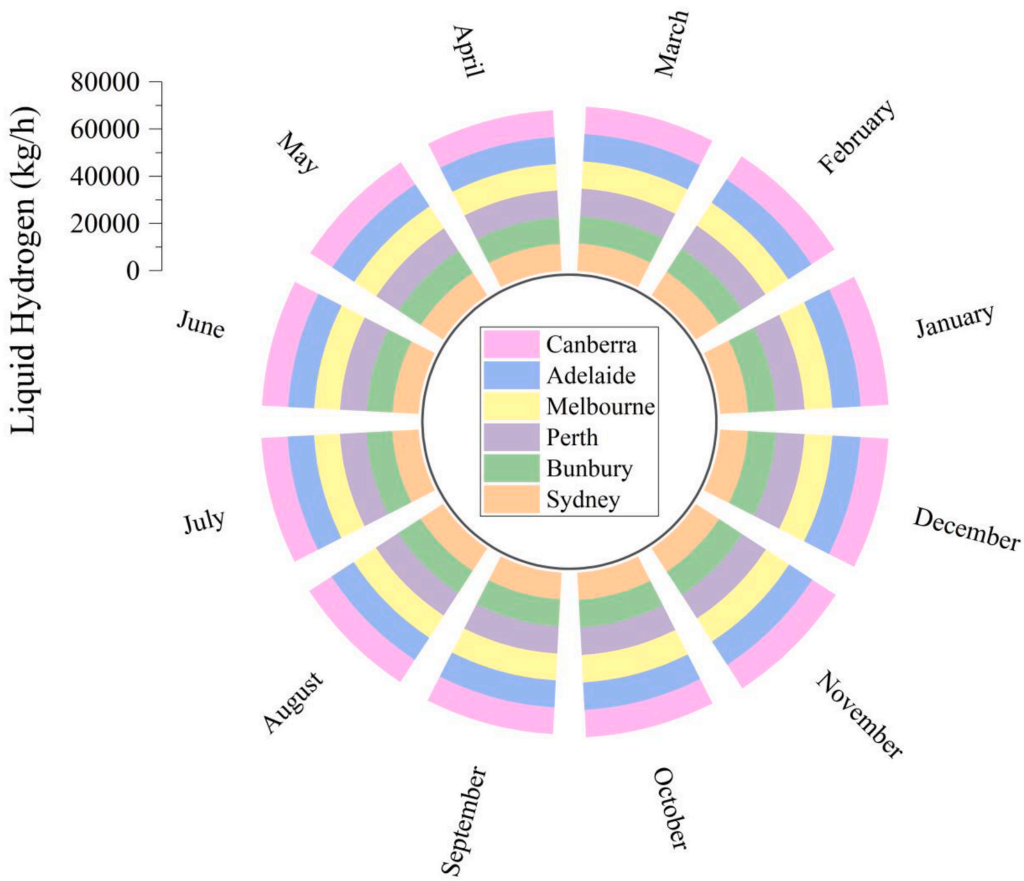

Fig. 13. Seasonal variation of liquid hydrogen storage in six selected Australian cities.

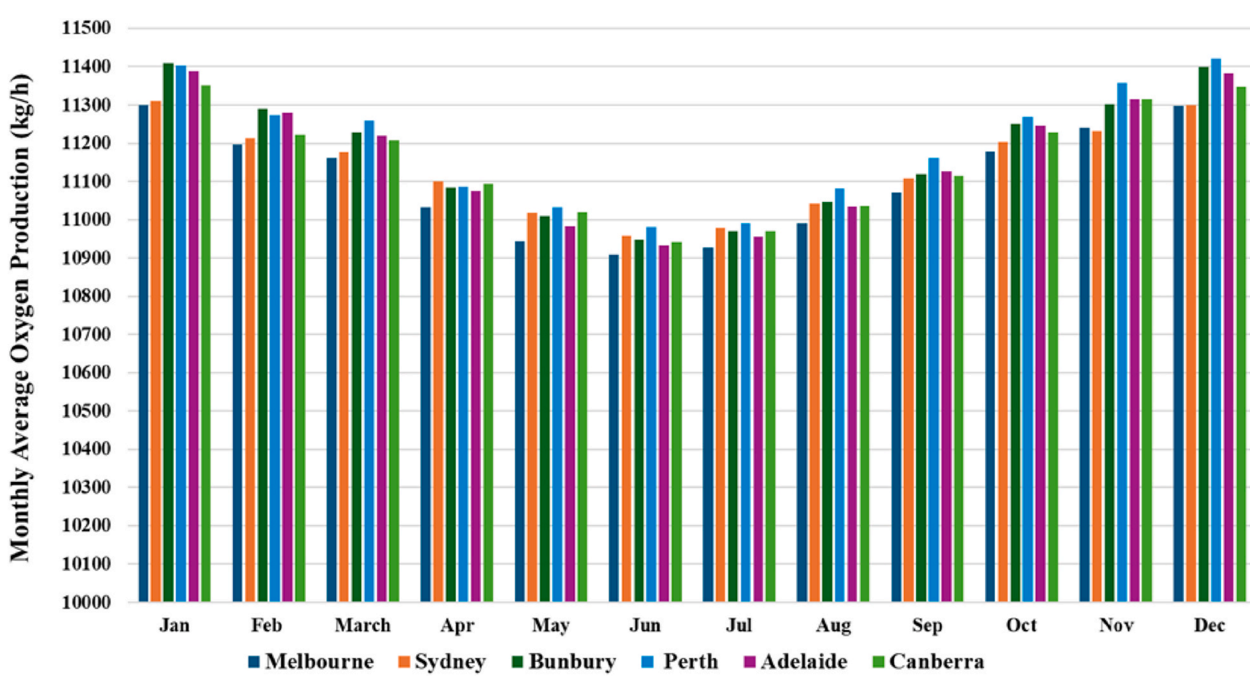

Fig. 14. Monthly oxygen production across six selected Australian cities.

cost across the six study cities, reflecting the explicit impact of solar irradiation and ambient temperature. Exergy efficiency peaked above 26 % in summer (December–February) and declined to 23–24 % in winter (June–August), while cost rates followed production trends, rising above 34,500 USD/h in summer and dropping below 32,500 USD/h in winter. Perth and Bunbury notably achieve higher efficiencies, albeit with increased costs, underscoring their strong solar resources. This performance trade-off confirms that elevated technical

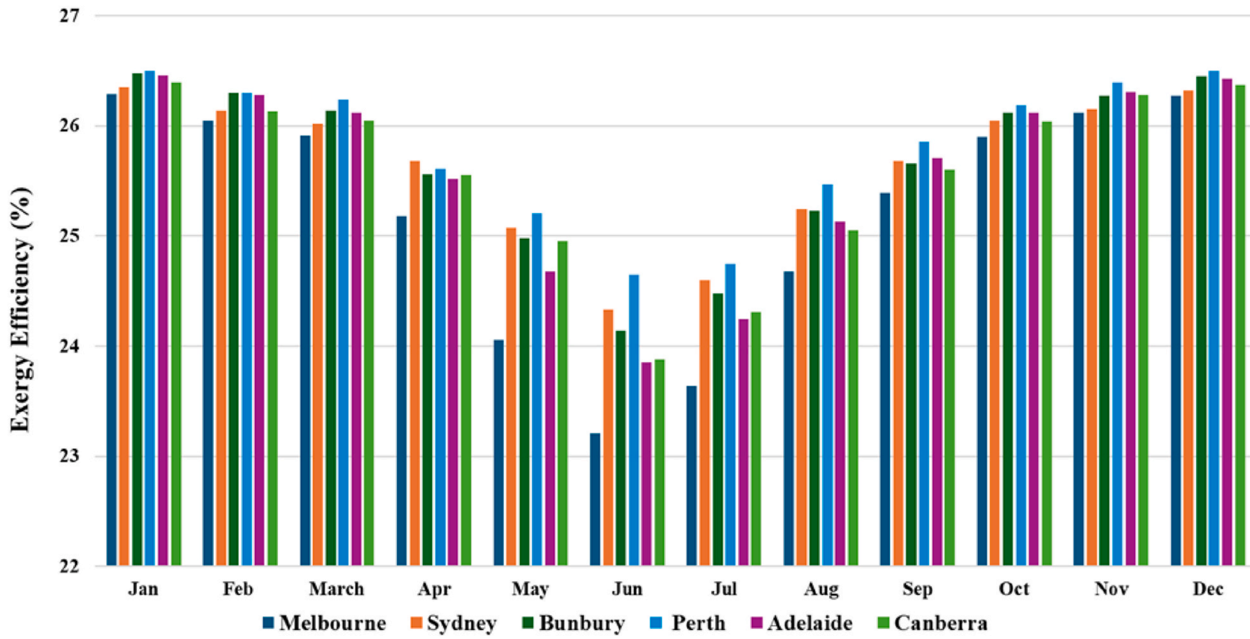

Fig. 15. Monthly exergy efficiency across six selected Australian cities.

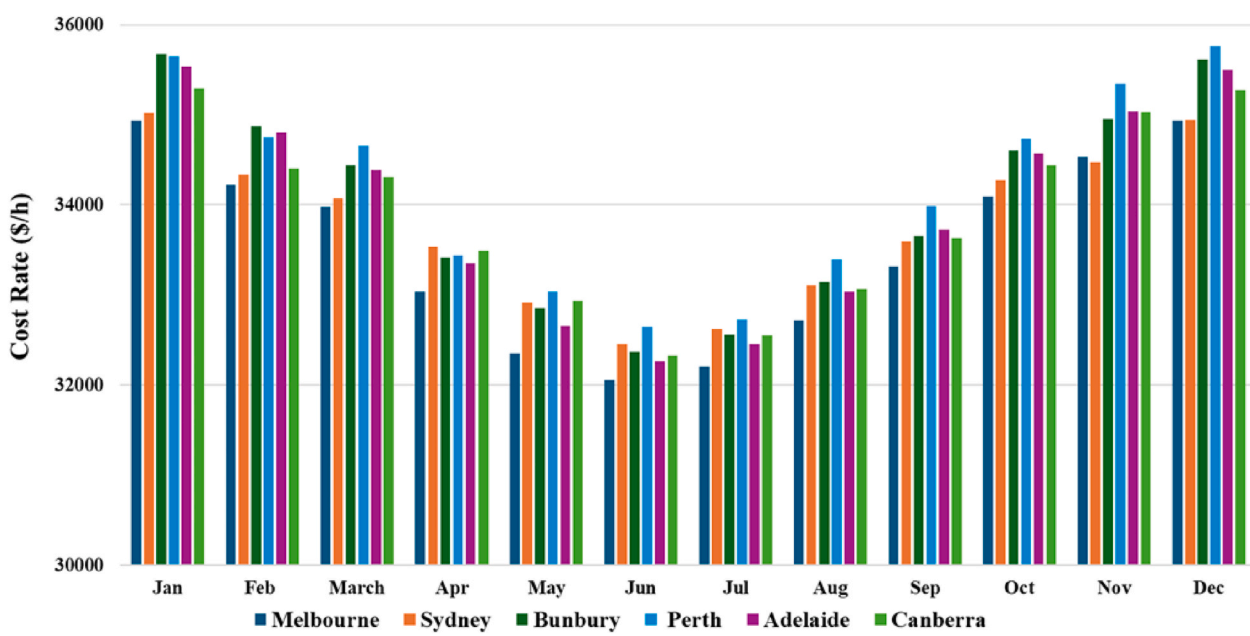

Fig. 16. Monthly cost rate across six selected Australian cities.

performance comes with economic implications. Similar findings have emerged in recent exergoeconomic studies of trigeneration systems, where enhancements in exergy efficiency also aligned with cost increases, highlighting a fundamental efficiency–cost coupling [87]. This reinforces the necessity of hybrid ANN–GA–TOPSIS optimization to identify operating conditions that strike a practical balance between performance and affordability, ensuring technical robustness and economic viability across varied Australian climates.

Table 10
Optimal values of objective functions from ANN–GA optimization.

Output	Unit	Case Study Cities					
		Melbourne	Sydney	Bunbury	Perth	Adelaide	Canberra
Power	kWh	863,085.6	942,055.2	993,621.6	788,565.6	920,390.4	902,311.2
Liquid H_2	kg/h	137,679.3	138,499.8	139,041	136,888.5	138,270.3	138,088.1
O_2	kg/h	133,642.4	134,052	134,322.8	133,246.5	133,937.4	133,846
Cost rate	USD/h	405,352.8	408,153.6	410,119.2	402,372	407,325.6	406,749.6

Beyond monthly dynamics, Table 10 summarizes the yearly performance across the six cities. Perth achieved the highest electricity generation (993,621.6 kWh), followed closely by Bunbury (942,055.2 kWh) and Adelaide (920,390.4 kWh), reflecting their stronger solar resource availability. However, liquid hydrogen production and oxygen generation showed relatively minor variation among cities, suggesting that once sufficient solar energy is available, the PEME subsystem provides stable conversion rates. Cost rates, however, differed more noticeably, with Perth again registering the highest due to its elevated throughput. These results underline the importance of site-specific deployment: locations with high irradiance yield greater energy and hydrogen outputs but require careful cost management strategies to maintain economic feasibility.

While these results confirm that system performance varies significantly with local solar resources, especially in Perth, Bunbury, and Adelaide, the benefits of the proposed system extend beyond technical outputs. To fully capture its contribution, it is also essential to evaluate the environmental advantages delivered through emission reductions and ecological offsets.

3.4.2. Environmental benefits

To quantify its impact on sustainability, the environmental performance of the proposed PTC–SRC–PEME configuration was analyzed, with particular attention to emission reduction and secondary benefits. Conventional fossil-fuel power plants emit approximately 0.4–1.0 t CO_2/MWh, depending on fuel type—about 0.8–1.05 t CO_2/MWh for coal and 0.4–0.55 t CO_2/MWh for natural gas, representing significant drivers of global warming and millions of premature deaths from outdoor air pollution [88]. By displacing this conventional generation, the proposed system achieves substantial greenhouse gas savings. Fig. 17 illustrates that CO_2 reductions peak during summer months (December–February), driven by higher solar irradiance and corresponding increases in power and hydrogen output; winter months exhibit smaller reductions. Among the six study cities, Perth and Bunbury lead in emissions avoided, consistent with their superior solar-based electricity production.

These avoided emissions translate into tangible economic and ecological benefits. According to Equation 22, each ton of CO_2 avoided can be valued at approximately 190 USD, based on the U.S. EPA's 2025 estimate for the Social Cost of Carbon under a 2 % discount rate [89].

$$\dot{C}_{Env} = \dot{C}_{CO_2} + \dot{m}_{CO_2} \tag{22}$$

Fig. 18 shows the monthly avoided environmental costs resulting from CO_2 reductions across the six study locations. The seasonal trend closely follows the emission reduction pattern shown in Fig. 17, with the highest cost savings achieved during summer months (December–February), exceeding 600 USD/tonCO_2 in Perth and Bunbury due to their higher solar irradiance and stronger system output. In contrast, winter months (June–August) show the lowest avoided costs, reflecting reduced solar input and smaller emission offsets. These outcomes highlight the potential of this system to deliver environmental and economic benefits, particularly in solar-rich regions.

Beyond monetary savings, the avoided carbon emissions can also be translated into ecological offsets, expressed as the equivalent expansion of green space. Using an average value of 4940 USD/hectare of non-waterfront bottomland areas [90], the proposed system delivers an offset of up to 0.12 ha per month, with clear seasonal variability linked to solar availability, as exhibited in Fig. 19. It illustrates that green space equivalents peak during summer months, particularly in Perth, Bunbury, and Adelaide, where higher irradiance drives greater emission reductions, while winter months correspond to smaller ecological gains. This reinforces the broader contribution of the system: in addition to producing hydrogen, oxygen, and electricity, it delivers tangible environmental co-benefits that align with urban greening and climate adaptation strategies. By quantifying benefits, it highlights how integrated solar–hydrogen systems can support sustainable energy transitions while simultaneously addressing environmental quality and resilience objectives.

3.5. Deployment prioritization and supply potential

Deployment priorities were determined by the locations that maximize system outputs most relevant to this study, liquid hydrogen, oxygen, and electricity, because all generated power is directed to electrolysis. Cities with higher annual electricity output from the solar–thermal subsystem also yield higher hydrogen and oxygen throughputs, improving both technical and economic feasibility. Based on the annual results, Bunbury, Perth, and Adelaide emerge as the most promising locations for initial deployment due to their high electricity production and correspondingly strong hydrogen and oxygen generation. As summarized in Table 11, their cost rates are comparable, confirming that output advantages are not offset by disproportionate operating expenses.

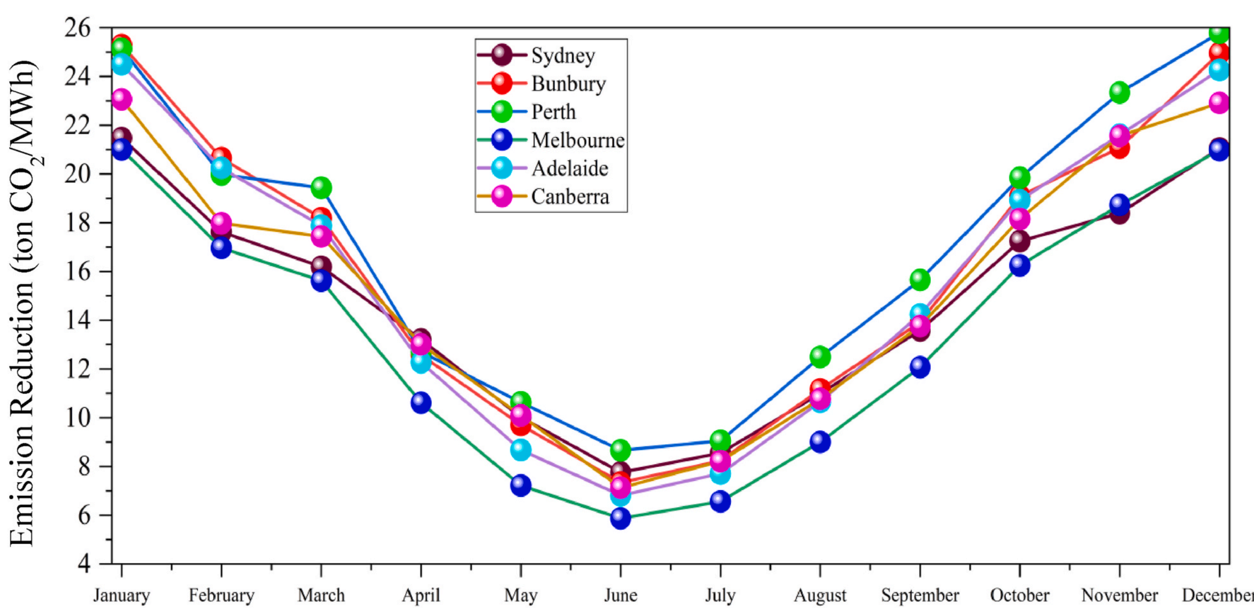

Fig. 17. Monthly CO_2 Emission across six selected Australian cities.

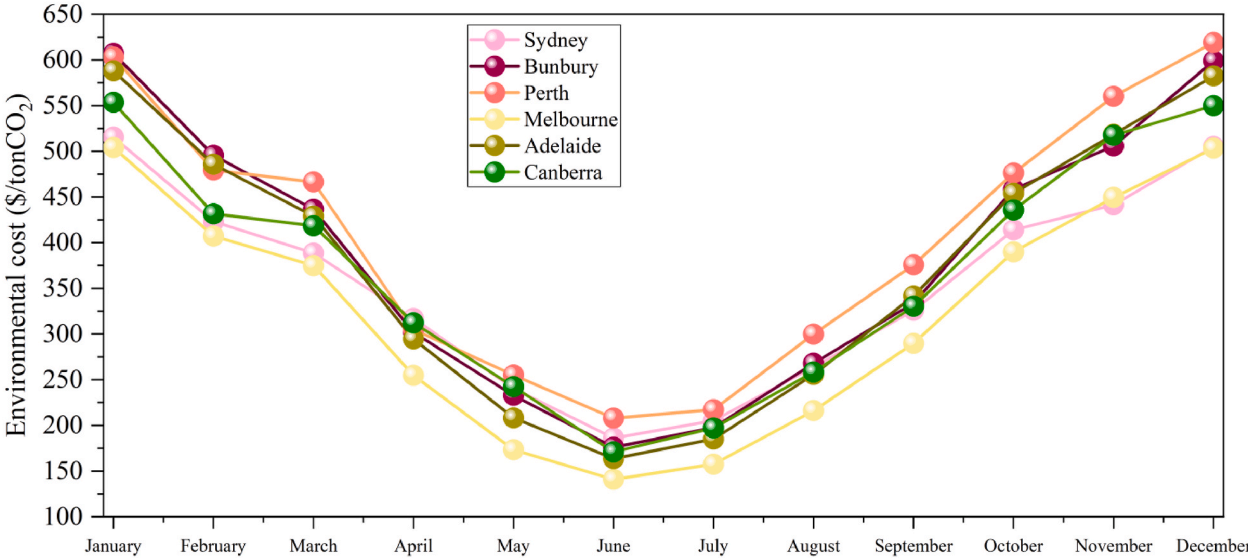

Fig. 18. Monthly avoided environmental costs from CO_2 reduction.

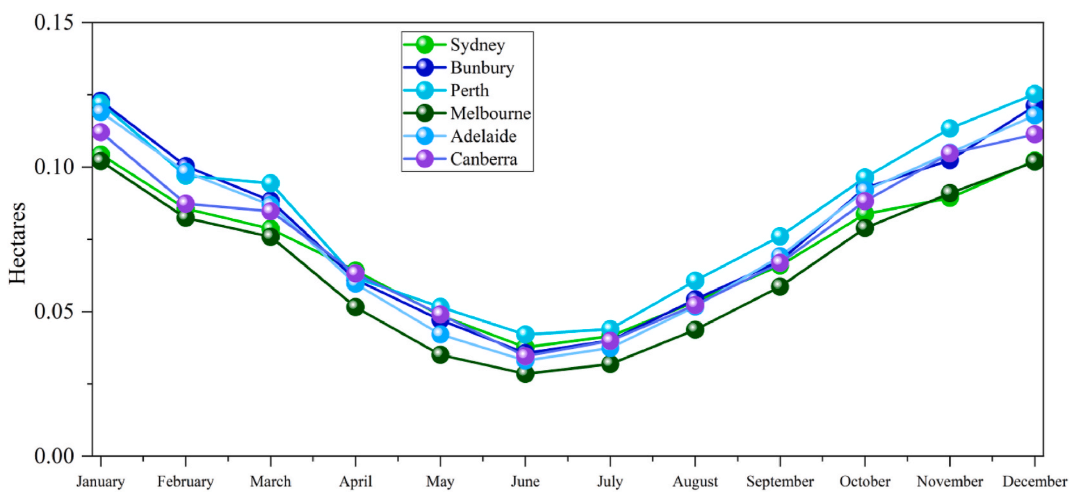

Fig. 19. Equivalent monthly increase in green space from avoided CO_2 emissions. (For interpretation of the references to colour in this figure legend, the reader is referred to the Web version of this article.)

Table 11
Annual system performance in the top candidate cities.

Output	Unit	Top Candidate Cities		
		Bunbury	Perth	Adelaide
Power	kWh	942,055.2	993,621.6	920,390.4
Liquid H_2	kg/h	138,499.8	139,041	138,270.3
O_2	kg/h	134,052	134,322.8	133,937.4
Cost rate	USD/h	408,153.6	410,119.2	407,325.6

To contextualize the scale of electricity output, Table 12 estimates the number of people whose annual electricity demand could be met by the system if power were delivered directly to end users rather than allocated to electrolysis. Following the benchmark of 1084 kWh per person per year [91,92], the served-population metric is computed as the ratio of annual electricity output to per-capita demand. While these served-population estimates are illustrative, since power is allotted to electrolysis for hydrogen and oxygen co-production, they offer a useful benchmark to communicate the scale of output to stakeholders.

Siting and permitting should prioritize Bunbury, Perth, and Adelaide, where stronger solar resources consistently enhance annual outputs. Because electricity is routed to electrolysis, electrolyzer sizing and

Table 12
Electricity supply potential per person (illustrative) [91,92].

Output	Unit	Case Study Cities					
		Melbourne	Sydney	Bunbury	Perth	Adelaide	Canberra
Annual Electricity Output	kWh/Year	431,839.9	688,536	624,218.3	580871.6	342621.1	279512.1
Assumed per-capita Electricity	kWh/Year	1084	1084	1084	1084	1084	1084
People Served	–	398	635	575	535	316	257

uptime are critical, with seasonal profiles indicating that surplus summer hydrogen can be directed to liquefaction and storage to balance winter shortages. The co-production of oxygen provides an additional revenue stream and sustainability benefit for local industry and health services, while off-take agreements can improve project bankability and reduce effective hydrogen costs. In regions with grid constraints, thermal and hydrogen storage can help smooth seasonal variability, while in stronger grids, opportunistic export and ancillary services can be pursued without compromising hydrogen supply. Finally, system costs remain dominated by the solar field, making collector efficiency improvements, maintenance optimization, and staged field expansion decisive factors for scaling. These deployment insights provide a foundation for examining the system's scalability and modularity in broader energy networks.

3.6. Scalability pathways and modular integration

The proposed configuration is inherently modular and mirrors evolving industry practice. Parabolic-trough collector fields are designed for phased expansion, added in blocks to increase thermal input and turbine output without reconfiguring the core cycle, a scalable strategy supported by recent studies of solar-hydrogen storage systems integrating thermal and electrical modules for improved energy management [93]. On the conversion side, electrolyzer capacity scales via additional PEM stacks and rectifiers operated in parallel, an approach compatible with commercial PEM skids and validated by the ANN-based performance correlations, aligned with the literature [94]. Storage is likewise extensible: liquid-hydrogen tankage and intermediate cold-box heat-exchange modules can be added to buffer seasonal surpluses, while high-pressure oxygen storage can be sized to match offtake contracts, aligning with multi-output electrolyzer system analyses that highlight the revenue and sustainability value of oxygen co-production. This block-wise approach supports staged capital deployment, operational redundancy, and maintainability; it also aligns with the ANN–GA–TOPSIS framework by re-optimizing setpoints (e.g., turbine pressure ratio, pinch points, collector count) after each capacity increment, preserving a balanced efficiency–cost profile as the plant grows.

Scalability limits are site-specific and centre on land, water, and infrastructure [95]. Collector fields require contiguous land with suitable solar access and low shading; siting near existing roads and transmission corridors reduces civil and interconnection costs [96]. Water availability and quality constrain electrolysis and cooling choices; where freshwater is limited, options include air-cooled condensers, wastewater reuse, or coupling with modest desalination sized to electrolyzer make-up rates [97]. Grid capacity, hydrogen logistics (liquefaction power, loading bays, safety setbacks), oxygen handling, and permitting for cryogenic storage set additional bounds. Despite these constraints, the system is well-positioned for global replication: its components are commercially mature, modular, and vendor-agnostic; controls can be standardized; and the climate-responsive optimization provides transferable sizing and dispatch rules for diverse irradiance and temperature regimes. Priority pathways for long-term deployment include (i) phased collector and PEM stack additions tied to contracted hydrogen and oxygen offtake, (ii) storage scaling to firm seasonal output, and (iii) co-location with industrial clusters or ports to leverage existing utilities and export infrastructure. Together, these strategies enable reproducible roll-outs from pilot to utility scale while maintaining technical robustness and bankability.

3.7. Comparison with prior studies

This section benchmarks the proposed PTC–SRC–PEME system against recently published solar-driven and hybrid hydrogen production studies to contextualize the findings of this research. The comparison, summarized in Table 13, highlights differences in system configurations, methodological approaches, and reported outcomes. By positioning the present work alongside prior studies, it becomes clear how its AI-based optimization, climate-responsive assessment, and integration of environmental co-benefits extend beyond the scope of earlier research.

Compared to earlier works, the present paper demonstrates a clear methodological advance by integrating climate-responsive site assessment into system design and optimization. Most previous studies applied generic modelling without considering the impact of local irradiance and temperature profiles on hydrogen production and co-generation

Table 13
Comparison with prior studies.

Ref	Core Configuration	Method Focus	Climate/Site Treatment	Reported Outcomes (Performance, Cost, Emissions)
Present Paper	PTC + SRC + PEM electrolyzer with liquid-H_2 & O_2 co-production	Multi-objective thermodynamic (EES), economic & AI-based optimization (ANN–GA–TOPSIS); deployment feasibility across climates	Six Australian cities (climate-responsive, site-specific irradiance and temperature effects assessed)	η_{En} = 30.83 %, η_{Ex} = 26.32 %, cost rate = 47.02 USD/h, Exergy Destruction = 4503 kWh; Solar and H_2 units dominate cost; CO_2 avoided ≈190 USD/ton, ≈0.12 ha/month green space; Perth, Bunbury & Adelaide are the best-performing sites.
[98]	PTC, ORC, CO_2 ejector refrigeration cycle with Heat Recovery Vapor Generator (HRVG) & recuperator	Thermodynamic modelling (energy/exergy) & economic (3E) assessment & cost minimization	Not specified (generic/steady-state modelling; no location-specific climate treatment mentioned)	η_{En} = 25.1 %, η_{Ex} = 12.67 %, Net power = 258.9 kW, total exergy destruction = 2333 kW, operational cost = 3.752 USD/h; emissions not reported.
[31]	Solar tower incorporated with TES to run steam methane reforming for H_2	Thermodynamic performance analysis using EES	Generic modelling, not climate-distinct	η_{En} (N.A.), η_{Ex} = 58 %, H_2 Output = 7.3 kg/s, cost data and emission not reported.
[99]	Solar-based multi-generation: CSP generating electricity & H_2	4E analysis (energy, exergy, economic, environmental) using thermodynamic modelling	Generic modelling (no climate-specific info)	η_{En} (N.A.), η_{Ex} = 13.5 %, H_2 Output = 5.15 kg/s, cost rate = 1301.85 USD/h & emission not reported.
[100]	CSP system for power & hydrogen	4E analysis (energy, exergy, economic, environmental) using thermodynamic modelling	Generic modelling	Solar-to-H_2 efficiency = 13.8 %, H_2 = 0.86 t/day or 0.01 kg/s; cost = USD/h 8.87/kgH_2 & emissions not specified.
[101]	CSP & s-CO_2 Brayton cycle for hydrogen	Energy & exergy analysis using thermodynamic modelling	Generic modelling; not site-specific	η_{En} = 30.5 %, η_{Ex} = 32.4 %, Solar field responsible for 48.2 % energy loss & 76.1 % exergy destruction; H_2 production = 3.52 mol/s or 0.0071 kg/s; cost & emissions not provided
[102]	Geothermal–solar hybrid with PEM electrolyzer & H_2 storage/consumption module	Thermodynamic daily simulation & demand–supply matching; parametric sensitivity (geothermal grade, Direct Normal Irradiance)	Seasonal/daytime variation explicitly modeled; community-level load profiles tested	ηEn = 13.28–14.36 %, η_{Ex} = N.A., daily H_2 production 306.24 kg or 0.00354 kg/s; exergy destruction in condensers/evaporators dominant; cost & emissions not reported

performance. In contrast, the current paper evaluated six distinct Australian climates, identifying optimal deployment locations (Perth, Bunbury, and Adelaide) and explicitly linking seasonal irradiance variations to hydrogen, oxygen, and electricity outputs, as well as to storage dynamics and avoided emissions. This approach enhances the practical relevance of results for real-world deployment.

In terms of performance metrics, this system demonstrated competitive performance (30.83 % energy efficiency and 26.32 % efficiency), higher than most CSP-driven hydrogen configurations except for the solar-tower reforming study [31], which reported exceptionally high exergy efficiency but without economic or emissions accounting. While cost rates in comparable CSP systems [98,99] were either much higher or reported at subsystem scales, the present work provides a plant-wide exergoeconomic evaluation, showing a balanced trade-off between efficiency and cost. Furthermore, its inclusion of environmental indicators, quantified CO_2 reduction (around 190 USD/ton) and green-space equivalence (≈0.12 ha/month), distinguishes it from prior studies, which often neglected emissions. Collectively, these contributions demonstrate the novelty and impact of this research in delivering an AI-driven, climate-adaptive, and environmentally grounded framework for hydrogen system deployment. Importantly, hydrogen remains the principal product of the system, with oxygen and electricity as valuable co-benefits, underscoring its role as a cornerstone of decarbonized energy pathways.

4. Limitations and future work

The findings are bounded by methodological and scope-related limitations. First, the EES model is steady-state; it does not capture fast transients, start-up/shut-down behavior, or part-load operation across the SRC–PEME–liquefaction units. Thus, dynamic control aspects like ramp rates, minimum up/down times, and seasonal degradation (e.g., collector soiling, gradual PEME efficiency loss) were not represented. In addition, the PEM electrolyzer was modeled using a simplified but empirically validated correlation that captures the nonlinear input–output relationship while omitting detailed electrochemical and degradation dynamics. Practical load limits (typically 25–120 % of rated capacity) were also not enforced, so shutdowns or penalties under off-design conditions were excluded from the economics. This approach, consistent with system-level studies and validated against experimental polarization data (Section 2.4.1, Fig. 6), necessarily abstracts fine-scale processes. Second, the ANN–GA surrogate and the TOPSIS decision layer were trained on data generated under idealized assumptions with equal weights on objectives. Weather inputs (from Meteonorm), discount rates, and the social cost of carbon were treated deterministically, while siting factors, such as land assembly, permitting timelines, and safety setbacks for Liquid Hydrogen (LH_2) and oxygen, were simplified. Third, the environmental assessment used a single emission factor for SMR and a stylized "green-space" equivalence; it omitted logistics-related emissions, such as liquefaction boil-off, transport, and export, as well as water sourcing impacts. Fourth, the architecture was fixed to PTC and SRC; alternative layouts (e.g., s-CO_2 Brayton topping, PV-assisted electrolysis, different thermal-storage schemes) and grid interactions (ancillary services, curtailment risk) are not co-optimized. Finally, while six Australian cities were analyzed to reflect climatic diversity, differences in grids, markets, and offtake conditions outside Australia were not modeled.

Future work will address these gaps with specific, practice-oriented advances. First, a multi-fidelity "digital twin" could integrate high-resolution dynamic models (PEME electrochemistry, LH_2 boil-off and cryogenics, turbine control) with the trained ANN, enabling Model Predictive Control (MPC) under real-time weather conditions. Higher-fidelity electrochemical models will also be adopted to refine efficiency and cost estimates, including the enforcement of practical PEME load windows (25–120 %). Second, distributionally robust and risk-aware optimization could be performed using weather ensembles and stochastic pricing, replacing the equal-weight TOPSIS method with Pareto-front navigation under defined uncertainty budgets. Third, co-designed water management systems could be introduced by integrating RO units or wastewater reuse, while optimizing the trade-off between pretreatment energy use and PEME lifetime. Dynamic degradation models will also be integrated to capture lifetime impacts of load fluctuations on PEME performance, ensuring more accurate cost estimates. Fourth, the system architecture could be extended to include hybrid PTC + s-CO_2 and PV-assisted electrolysis by running automated architecture searches to quantify the added value of alternative cycles. Fifth, market-coupled offtake optimization could embed co-optimization of hydrogen, oxygen, and ancillary services, incorporating contract-aware storage and bankability constraints (e.g., debt-service coverage, take-or-pay agreements). Sixth, Geographic Information System (GIS)-based siting analysis could be combined with Quantitative Risk Assessment for LH_2/O_2 to deliver permit-ready layouts reflecting land shading, transmission access, and safety zones. Finally, a forward-looking life-cycle techno-economic assessment could include learning curves, component degradation, and logistics emissions, producing location-specific LCH/Oxygen estimates and comparing export pathways, such as LH_2. These advances will turn the present climate-responsive optimization into an operational, finance-grade toolchain centered on hydrogen, while rigorously capturing dynamics, uncertainty, infrastructure, and market realities.

5. Conclusion

This paper presents the development of a solar-powered multi-generation setup that combines Parabolic Trough Collectors (PTC), a Steam Rankine Cycle (SRC), and a Proton Exchange Membrane Electrolyzer (PEME) to produce liquid hydrogen, oxygen, and electricity in an efficient, scalable, and climate-responsive manner. Engineering Equation Solver (EES) was employed for thermodynamic modelling, while a hybrid Artificial Neural Network (ANN)–Genetic Algorithm (GA) framework in Statistica, joined with Technique for Order Preference by Similarity to Ideal Solution (TOPSIS) decision support, enabled multi-objective optimization.

The Key conclusions are as follows.

1. **System performance:** The optimal configuration achieved an energy efficiency of 30.83 % and exergy efficiency of 26.32 % at a total cost of 47.02 USD/h, with the solar field contributing the largest share of both cost (38.17 USD/h) and exergy destruction (3364 kWh).
2. **Location-specific outputs:** Location-resolved analysis showed that Perth, Bunbury, and Adelaide achieved the highest annual hydrogen and power outputs, driven by superior solar irradiance, with outputs peaking in summer.
3. **Environmental benefits:** The system avoided approximately 190 USD/ton of CO_2 emissions, equivalent to 0.12 ha/month of green-space value, quantifying tangible sustainability impacts.
4. **Economic feasibility:** Co-production of electricity and oxygen alongside hydrogen improved system economics, supporting integration into broader energy systems.
5. **Trade-offs identified:** Efficiency improvements were linked to higher costs, with feasible solutions clustering around intermediate efficiency–cost trade-offs, highlighting practical design boundaries.

Novelty lies in delivering a climate-responsive, multi-city analysis that integrates PTC–SRC with PEM electrolysis in a finance-aware, AI-driven framework, linking techno-economic outcomes with quantified environmental value and multi-output synergies. Future work will extend this framework with digital twins, dynamic uncertainty-aware optimization, and Geographic Information System (GIS)-based siting for practical development.

CRediT authorship contribution statement

Ehsanolah Assareh: Writing – original draft, Visualization, Validation, Software, Methodology, Investigation, Formal analysis, Data curation, Conceptualization. **Behzad Rismanchi:** Writing – review & editing, Supervision, Resources, Methodology. **Nima Izadyer:** Writing – review & editing, Writing – original draft, Visualization, Supervision, Project administration, Methodology, Investigation. **Ali Bedakhanian:** Writing – original draft, Investigation, Data curation. **Elmira Jamei:** Software, Resources, Methodology. **Jagadeesh Kumar Alagarasan:** Writing – review & editing, Supervision, Investigation.

Declaration of generative AI

The authors applied OpenAI and Grammarly software to improve the clarity and readability of the manuscript. All content was subsequently checked and revised by the authors, and they accept full responsibility for the ultimate version. The tool was employed only for language refinement and did not replace the authors' intellectual or analytical contributions.

Declaration of competing interest

The authors declare that they have no known competing financial interests or personal relationships that could have appeared to influence the work reported in this paper.

References

[1] International Energy Agency (IEA). Growth in global energy demand surged in 2024 to almost twice its recent average. Available from: https://www.iea.org/news/growth-in-global-energy-demand-surged-in-2024-to-almost-twice-its-recent-average; 2024.
[2] International Energy Agency (IEA). World energy outlook 2024 – executive summary. 2024.
[3] MSCI Sustainability Institute. Global electricity generation in 2023. MSCI Sustainability Institute; 2023. Available from: https://www.msci-institute.com/charts/global-electricity-generation-in-2023/.
[4] Bhuiyan MMH, Siddique Z. Hydrogen as an alternative fuel: a comprehensive review of challenges and opportunities in production, storage, and transportation. Int J Hydrogen Energy 2025;102:1026–44.
[5] International Energy Agency (IEA). GHG emissions of hydrogen and its derivatives. In: Global Hydrogen Review 2024; 2024. Paris.
[6] Filonchyk M, et al. Greenhouse gases emissions and global climate change: examining the influence of CO2, CH4, and N2O. Sci Total Environ 2024:173359.
[7] Kiehbadroudinezhad M, Merabet A, Hosseinzadeh-Bandbafha H. Health impacts of greenhouse gases emissions on humans and the environment. In: Advances and technology development in greenhouse gases: emission, capture and conversion. Elsevier; 2024. p. 265–91.
[8] Abdul-Nabi SS, et al. Climate Change and its Environmental and Health Effects from 2015 to 2022: a scoping review. Heliyon 2025;11:e42315.
[9] Sebbagh T, Şahin ME, Beldjaatit C. Green hydrogen revolution for a sustainable energy future. Clean Technol Environ Policy 2024;26(12):4017–40.
[10] Maka AO, Mehmood M. Green hydrogen energy production: current status and potential. Clean Energy 2024;8(2):1–7.
[11] Segovia-Hernández JG, et al. Green hydrogen production for sustainable development: a critical examination of barriers and strategic opportunities. RSC Sustain 2025;3(1):134–57.
[12] Habib MA, et al. Hydrogen combustion, production, and applications: a review. Alex Eng J 2024;100:182–207.
[13] Anand C, et al. Green hydrogen for a sustainable future: a review of production methods, innovations, and applications. Int J Hydrogen Energy 2025;111:319–41.
[14] Li X, et al. A critical review on integrated system design of solar thermochemical water-splitting cycle for hydrogen production. Int J Hydrogen Energy 2022;47(79):33619–42.
[15] Majumdar A, et al. Control and control-oriented modeling of PEM water electrolyzers: a review. Int J Hydrogen Energy 2023;48(79):30621–41.
[16] Gong J, et al. Response behaviour of proton exchange membrane water electrolysis to hydrogen production under dynamic conditions. Int J Hydrogen Energy 2023;48(79):30642–52.
[17] Bin S, et al. High-pressure proton exchange membrane water electrolysis: current status and challenges in hydrogen production. Int J Hydrogen Energy 2024;67:390–405.
[18] Ranz M, et al. Dynamics of anion exchange membrane electrolysis: unravelling loss mechanisms with electrochemical impedance spectroscopy, reference electrodes and distribution of relaxation times. J Power Sources 2024;605:234455.
[19] Gao J, et al. Recent advances in anion exchange membranes. Chin J Struct Chem 2025;44(5):100563.
[20] Zhang Y, et al. Optimization of multiple alkaline water electrolyzers coupled with solar photovoltaic power for green hydrogen production on a large scale. Int J Hydrogen Energy 2025;136:511–32.
[21] Yan J, et al. Advancing solar-powered hydrogen generation: a comparative analysis of efficiency, emissions, and economic viability. Int J Hydrogen Energy 2025;131:255–72.
[22] Singh SK, Tiwari AK. Solar-powered hydrogen production: advancements, challenges, and the path to net-zero emissions. Int J Hydrogen Energy 2024;84:549–79.
[23] Hajjaji M, et al. Techno-economic and environmental evaluation of on-site solar hydrogen systems for decarbonizing port in Corsica. Int J Hydrogen Energy 2025;134:229–40.
[24] Hossain S, et al. The role of solar thermal hydrogen production technologies in future energy solutions: a review. Energy Convers Manag X 2025:100876.
[25] Aravindan M, Kumar P. Hydrogen towards sustainable transition: a review of production, economic, environmental impact and scaling factors. Results Eng 2023;20:101456.
[26] Soni N, Reddy K. Techno-economic assessment of concentrated solar power technologies integrated with thermal energy storage system for green hydrogen production. Int J Hydrogen Energy 2024;72:1184–203.
[27] Park J, et al. Techno-economic analysis of solar powered green hydrogen system based on multi-objective optimization of economics and productivity. Energy Convers Manag 2024;299:117823.
[28] Kumar S, Kumar KR. Techno economic feasibility study on hydrogen production using concentrating solar thermal technology in India. Int J Hydrogen Energy 2022;47(89):37708–23.
[29] Zhang T, et al. A systematic review of modelling methods for studying the integration of hydrogen into energy systems. Renew Sustain Energy Rev 2025;208:114964.
[30] Soyturk G, et al. Dynamic analysis and multi-objective optimization of solar and hydrogen energy-based systems for residential applications: a review. Int J Hydrogen Energy 2024;75:662–89.
[31] Alaidaros A, AlZahrani AA. Integrated solar system for hydrogen production using steam reforming of methane. Int J Hydrogen Energy 2025;140:1033–48.
[32] Raja IB, et al. Regional variability in the performance of Solar-Green Hydrogen Hybrid Energy Systems (SGHHES): synergistic enviro-economic analysis andevaluation across six climatic zones using multi-criteria decision analysis. Int J Hydrogen Energy 2025;138:681–93.
[33] Vethamani AB, Thangavel V. Climatic effects on solar-driven HHO production: an experimental insight. Int J Hydrogen Energy 2025;119:283–93.
[34] Gutiérrez-Martín F, et al. Modeling and simulation of integrated solar PV-hydrogen systems. Int J Hydrogen Energy 2024;52:995–1006.
[35] Australian National University. Efficient solar hydrogen generation. Canberra, Australia: Final Report; 2023.
[36] CSIRO. CSIRO solar thermochemical hydrogen R&D Mid-Project report. Canberra, Australia: Commonwealth Scientific and Industrial Research Organisation (CSIRO); 2020.
[37] Şahmerdan O, et al. Thermodynamic analysis of different nanofluids in a parabolic trough solar collector for hydrogen production. Int J Hydrogen Energy 2025;144:875–86.
[38] Alirahmi SM, et al. Development and multi-criteria optimization of a solar thermal power plant integrated with PEM electrolyzer and thermoelectric generator. Int J Hydrogen Energy 2022;47(57):23919–34.
[39] Sathish T, et al. An absorber of parabolic trough collector for hydrogen production in a solid oxide fuel cell. Fuel 2023;343:127982.
[40] Singh SK, Das AK, Dixit AR. Performance of proton exchange membrane in solar-integrated Kalina cycle systems for green hydrogen production. Therm Sci Eng Prog 2025;60:103413.
[41] Razmi AR, et al. A green hydrogen energy storage concept based on parabolic trough collector and proton exchange membrane electrolyzer/fuel cell: thermodynamic and exergoeconomic analyses with multi-objective optimization. Int J Hydrogen Energy 2022;47(62):26468–89.
[42] Zhang S, Zhang N. Review on integrated green hydrogen polygeneration system——electrolysers, modelling, 4 E analysis and optimization. J Clean Prod 2023;414:137631.
[43] Fang Z, et al. Performance evaluation and multi-objective optimization of a solar-thermal-assisted energy system: supercritical CO2 Brayton cycle and solid oxide electrolysis/fuel cells. Energy Convers Manag 2024;308:118404.
[44] Chen W, Ren H, Zhou W. Review of multi-objective optimization in long-term energy system models. Global Energy Interconnection 2023;6(5):645–60.
[45] Song Y, et al. Multi-objective optimization and long-term performance evaluation of a hybrid solar-hydrogen energy system with retired electric vehicle batteries for off-grid power and heat supply. Int J Hydrogen Energy 2024;62:867–82.
[46] Han Z, et al. Multi-objective sustainability optimization of a solar-based integrated energy system. Renew Sustain Energy Rev 2024;202:114679.
[47] Zhu X, et al. Multi-objective optimization of a hybrid energy system integrated with solar-wind-PEMFC and energy storage. J Energy Storage 2023;72:108562.
[48] Assareh E, et al. Optimizing solar-powered multi-generation systems for sustainable energy management in university buildings using Neural Networks and Genetic Algorithms. J Build Eng 2025:112939.

[49] Shahverdi N, Saffari A, Amiri B. A systematic review of artificial intelligence and machine learning in energy sustainability: research topics and trends. Energy Rep 2025;13:5551–78.
[50] Ukoba K, et al. Optimizing renewable energy systems through artificial intelligence: review and future prospects. Energy Environ 2024;35(7):3833–79.
[51] Kazemi H, Lotfollahi A, Moghimi M. A net-zero carbon emission multi-generation system for green ammonia production: comprehensive analysis and ANN-assisted optimization using moth flame optimizer. Int J Hydrogen Energy 2025;137:303–22.
[52] Yilmaz C, et al. Thermal design and genetic algorithm optimization of geothermal and solar-assisted multi-energy and hydrogen production using artificial neural networks. Energy 2025;324:135941.
[53] Hamida MBB, et al. Dynamic optimization of a solar–sCO2–CAES hybrid energy system: integration of green hydrogen production and AI-based energy management. Int J Hydrogen Energy 2025;146:149888.
[54] Zhou W, Lin Y. Optimization and 4E analysis of a hybrid solar-methane System for hydrogen and freshwater production with enhanced waste heat recovery from compressed air energy storage System. Energy 2025:134994.
[55] Alirahmi SM, Rostami M, Farajollahi AH. Multi-criteria design optimization and thermodynamic analysis of a novel multi-generation energy system for hydrogen, cooling, heating, power, and freshwater. Int J Hydrogen Energy 2020;45(30):15047–62.
[56] Wei H, Hasanuzzaman M, Selvaraj J. Decision study and ANN-assisted multi-criteria optimization of a novel three-state solar-driven integrated process using energy storage for hydrogen liquefication: a case study for Malaysian solar status. J Energy Storage 2024;99:113216.
[57] Sami S, Gholizadeh M, Deymi-Dashtebayaz M. An applicable multi-generation system for different climates from energy, exergy, exergoeconomic, economic, and environmental (5E) perspectives. Sustain Cities Soc 2024;100:105057.
[58] United Nations (UN). Sustainable Development Goals 2015. Available from: https://sdgs.un.org/goals.
[59] Dincer I, Rosen MA. Exergy: energy, environment and sustainable development. Newnes; 2012.
[60] Michaelides E. Exergy analysis for energy conversion systems. Cambridge University Press; 2021.
[61] Yüksel YE. Thermodynamic assessment of modified Organic Rankine Cycle integrated with parabolic trough collector for hydrogen production. Int J Hydrogen Energy 2018;43(11):5832–41.
[62] Kalogirou SA. Solar energy engineering: processes and systems. Elsevier; 2023.
[63] Assareh E, Alirahmi SM, Ahmadi P. A sustainable model for the integration of solar and geothermal energy boosted with thermoelectric generators (TEGs) for electricity, cooling and desalination purpose. Geothermics 2021;92:102042.
[64] Ishaq H, Dincer I, Naterer G. Development and assessment of a solar, wind and hydrogen hybrid trigeneration system. Int J Hydrogen Energy 2018;43(52):23148–60.
[65] Karapekmez A, Dincer I. Thermodynamic analysis of a novel solar and geothermal based combined energy system for hydrogen production. Int J Hydrogen Energy 2020;45(9):5608–28.
[66] Ioroi T, et al. Thin film electrocatalyst layer for unitized regenerative polymer electrolyte fuel cells. J Power Sources 2002;112(2):583–7.
[67] Kianfard H, Khalilarya S, Jafarmadar S. Exergy and exergoeconomic evaluation of hydrogen and distilled water production via combination of PEM electrolyzer, RO desalination unit and geothermal driven dual fluid ORC. Energy Convers Manag 2018;177:339–49.
[68] Boyaghchi FA, Chavoshi M, Sabeti V. Multi-generation system incorporated with PEM electrolyzer and dual ORC based on biomass gasification waste heat recovery: exergetic, economic and environmental impact optimizations. Energy 2018;145:38–51.
[69] Szargut J, Morris DR, Steward FR. Exergy analysis of thermal, chemical, and metallurgical processes. 1987.
[70] Assad M, Rosen MA. Design and performance optimization of renewable energy systems. Academic press; 2021.
[71] SolarGIS. Maps and GIS data. Available from: https://solargis.com/resources/free-maps-and-gis-data?locality=australia-and-oceania; 2025 9 September 2025.
[72] Ag M. Meteonorm Version 8. Bern, Switzerland: Meteotest AG; 2020.
[73] Falcão D, Pinto A. A review on PEM electrolyzer modelling: guidelines for beginners. J Clean Prod 2020;261:121184.
[74] The MathWorks I. Matlab. MathWorks. Massachusetts, USA: Natick; 2022.
[75] Yates JK. Engineering economics. CRC Press; 2016.
[76] De Cata D, et al. Electrified steam methane reforming as efficient pathway for sustainable hydrogen production and industrial decarbonization: a critical review. Int J Hydrogen Energy 2025;105:31–44.
[77] Abed N, et al. Assessment and evaluation of the thermal performance of various working fluids in parabolic trough collectors of solar thermal power plants under non-uniform heat flux distribution conditions. Energies 2020;13(15):3776.
[78] Bellos E, Tzivanidis C, Antonopoulos KA. A detailed working fluid investigation for solar parabolic trough collectors. Appl Therm Eng 2017;114:374–86.
[79] TIBCO Software Inc. Statistica. Palo Alto, CA: TIBCO Software Inc.; 2023.
[80] Liu Y, et al. Optimization and analysis of solar-driven biomass gasification using a CFD-ANN-GA framework. Energy 2025;325:136036.
[81] Goh QH, et al. Modelling and multi-objective optimisation of sustainable solar-biomass-based hydrogen and electricity co-supply hub using metaheuristic-TOPSIS approach. Energy Convers Manag 2023;293:117484.
[82] Bai Y, Wang B, Cheng L. A comprehensive thermodynamic, economic, and environmental analysis of a novel parabolic trough solar-driven multigeneration system for generating power, hydrogen, and freshwater. Process Saf Environ Prot 2024;184:227–47.
[83] Mansir IB, Abubakar Z, Chaturvedi R. Performance and exergoeconomic evaluation of a parabolic trough-based hybrid power system with LNG expansion and electrolytic hydrogen generation. Int J Hydrogen Energy 2025;147:150004.
[84] Babay M-A, et al. Forecasting green hydrogen production: an assessment of renewable energy systems using deep learning and statistical methods. Fuel 2025;381:133496.
[85] Superchi F, et al. Towards sustainable energy independence: a case study of green hydrogen as seasonal storage integration in a small island. Renew Energy 2025;245:122813.
[86] Bo Z, et al. A review of oxygen generation through renewable hydrogen production. Sustain Chem Clim Action 2025:100079.
[87] Khalid F, Suhail SA, Akbulut U. In-depth exergoeconomic analysis and optimization of a solar-wind hybrid trigeneration system for green hydrogen, power, and cooling. Int J Hydrogen Energy 2025;143:1174–85.
[88] Romanello M, et al. The 2023 report of the Lancet Countdown on health and climate change: the imperative for a health-centred response in a world facing irreversible harms. Lancet 2023;402(10419):2346–94.
[89] Resources for the Future. EPA values for the social cost of greenhouse gases. Available from: https://costofcarbon.org/epa-values-for-the-social-cost-of-greenhouse-gases; 2023 10 September 2025.
[90] Brander L, et al. Economic values for ecosystem services: a global synthesis and way forward. Ecosyst Serv 2024;66:101606.
[91] U.S. energy Information administration. Washington, DC, USA: International Energy Outlook 2023; 2023.
[92] U.S. Energy Information Administration. International Electricity Consumption Data [cited 2025 September 10]; Available from: https://www.eia.gov/international/data/world/electricity/electricity-consumption; 2023.
[93] Liu Z, et al. A review of hydrogen production through solar energy with various energy storage devices. Int J Hydrogen Energy 2025;144:932–46.
[94] El-Hamalawy AF, Farag HE, Asif A. Multi-objective optimal modular design of PEM electrolyzers for efficient and scalable green hydrogen production plants. J Power Sources 2025;637:236510.
[95] Tonelli D, et al. Global land and water limits to electrolytic hydrogen production using wind and solar resources. Nat Commun 2023;14(1):5532.
[96] Cheng C, et al. High-Resolution siting of utility-scale solar and wind: bridging pixel-level costs and regional planning. Energies 2025;18(16):4361.
[97] Arthur T, et al. Renewable hydrogen production using non-potable water: thermal integration of membrane distillation and water electrolysis stack. Appl Energy 2023;333:120581.
[98] Ogaili HH, et al. Energy, exergy, and economic performance analysis of integrated parabolic trough collector with organic rankine cycle and ejector refrigeration cycle. Energy Convers Manag X 2025;25:100843.
[99] Qing X. Solar-driven multi-generation system: thermoeconomic and environmental optimization for power, cooling, and liquefied hydrogen production. Energy 2024;293:130409.
[100] Muhammad HA, et al. Solar hydrogen production: technoeconomic analysis of a concentrated solar-powered high-temperature electrolysis system. Energy 2024;298:131284.
[101] Sun X, et al. Energy and exergy analysis of a novel solar-hydrogen production system with S–I thermochemical cycle. Energy 2023;283:128737.
[102] Liu G, Ji D, Qin Y. Geothermal-solar energy system integrated with hydrogen production and utilization modules for power supply-demand balancing. Energy 2023;283:128736.